DEPARTMENT OF THE INTERIOR
U.S. GEOLOGICAL SURVEY

Venus: Quantitative Analyses of Terrain Units Identified from Venera 15/16 Data and Described in Open-File Report 90-24

by

Gerald G. Schaber[1]

Open-File Report 90-468
1990

Prepared for the National Aeronautics and Space Administration
Under NASA Contracts W15,415 and WO8,777

[1] 2255 N. Gemini Drive
Flagstaff, Arizona 86001

TABLE OF CONTENTS

LIST OF FIGURES

LIST OF TABLES

INTRODUCTION

The Venera 15 and 16 spacecraft provided radar-image and altimetric data of sufficient radar cell resolution (1.5- 2.5 km) to permit compilation of pre-Magellan maps of regional geologic/geomorphic terrains and structural elements within 111.4 X 10^6 km^2 of the northern quarter of Venus (Sukhanov et al., 1989; Schaber and Kozak, 1990). Pioneer-Venus and Earth-based radar data provided a significant amount of additional information for part of the mapped area. The present report describes digital correlations and analyses of various physical aspects of the mapped terrain units described in Schaber and Kozak (1990) and was prepared to be used in conjunction with that report.

The interrelations of the geologic/geomorphic terrain units and terrain groups presented here are based primarily on analyses of pre-Magellan radar images and altimetric data. Therefore, these data and the correlations made among them, including densities of suspected impact craters, should be taken as tentative prior to verification or rejection based on a thorough analysis of higher resolution Magellan data. The current results are provided here primarily as a guide to future investigations by Magellan teams and by the planetary geoscience community at large.

METHODS

The contacts between the 34 different geologic/geomorphic terrain units mapped by Schaber and Kozak (1990 Plate 1) were digitized and converted to a Sinusoidal Equal-Area projection. The projection was then registered with a merged Pioneer Venus/Venera 15/16 altimetric database (E. Eliason and P. Ford, oral communications, 1990), root mean square (rms) slope values (C-power$^{-1/2}$), and radar reflectivity (rho) values derived from Pioneer Venus (Pettengill et al., 1980, 1988). The resulting information, shown here principally in tables and graphs, includes comparisons of individual terrain units (Table 1) and the terrain groups to which they are assigned (Table 2; Figs. 1-12) in regard to percentage of the map area covered, elevation, rms slopes, reflectivity, and density of suspected impact craters >10 km in diameter and their latitudinal and longitudinal variations (Tables 3-5; Figs. 13-34). [The concept of terrain groups did not figure in Schaber and Kozak (1990), but it is useful here because of the difficulty in portraying the areal distribution of the thirty-four terrain units in page-size black and white illustrations]. The areal distribution of individual terrain units, as well as the location of features named in this report, is given on Plate 1 and Table 1 of Schaber and Kozak (1990).

AREAL DISTRIBUTION OF TERRAIN MATERIALS

The percentages of map area covered by individual terrain units and terrain groups, respectively, are shown in Figures 13 and 14. The high and low marginal belt groups and the hilly

terrain group each consist of a single terrain unit. Smooth plains (unit ps), intermediate plains (unit pi), mottled plains (unit pm), complex plains (unit pc), and domical hill or hill field (unit dh) units form the lowland plains terrain group, which covers 52.6% of the mapped area. (Domical hill or hill field terrain (unit dh) is here included in the lowland plains group because of the unit's obvious genetic association with plains situated at or near the mean planetary radius; see below.)

The smooth plains unit alone covers 30.0% of the mapped area but is present in only minor amounts between lat 20° and 90° N, long 0° and 150° (Fig. 1b). This region is dominated instead by more complex plains units, lineated terrains, and tesserae. The three most areally extensive groups following the lowland plains group are the lineated and fractured terrain group (14.9% of map area), the tessera group (9.6%) and the ridged terrain group (9.0%). The upland plains group, consisting of tessera-mantling plains (unit pt) and smooth plains of Lakshmi Planum (unit psl), covers only 4.8% of the map area. Combined, the groups noted above cover about 91% of the area mapped within the northern quarter of the planet.

HYPSOMETRY

Elevation values included in this report are radial distances to the center of mass of Venus computed during the digital processing and merging of Pioneer Venus and Venera 15/16 spacecraft altimetry databases (E. Eliason and P. Ford, oral communications, 1990). The mean planetary radius (MPR), the datum, used here is 6051.9 km as derived by Ford (1986) from Pioneer Venus data. Elevations of terrain units described below are given in Figure 15 and Table 3; elevations of terrain groups, in Figure 16 and Table 4.

The relation of the percentages of area to specific elevations were determined through a hypsometric analysis of the merged Pioneer Venus and Venera 15/16 altimetry database coinciding with the mapped part of the northern quarter of Venus (Fig. 17). The hypsometric curve of the mapped region is highly unimodal. A similar situation was shown to be true for Venus on a global basis following analysis of the entire Pioneer Venus altimetric database (Masursky et al., 1980; Pettengill et al., 1980). Because ocean basins are absent on Venus, the large areal extent of the lowland plains terrain group strongly influences the location and peakedness of the hypsometric curve. (All five terrain units of the lowland plains group have mean elevations that lie below the MPR.)

The only highly elevated smooth plains unit, smooth plains of Lakshmi Planum (unit psl), forms the surface of the Lakshmi plateau and is about 3.0 km above the MPR. Tessera-mantling plains (unit pt) has a mean elevation about 1 km above the MPR.

Lakshmi-type marginal belt terrain (unit ml) is the only unit in the high marginal belt group. It forms major linear belts of mountains (e.g., Maxwell, Freja, and Akna Montes) that nearly surround Lakshmi Planum. These mountains dominate the landscape

in the northern quarter of Venus. The unit has a mean elevation of 6056.57±2.28 km, which is 4.7 km above the MPR, and reaches its maximum elevation of about 11.5 km at the summit of Maxwell Montes. Tessera-type marginal belt terrain (unit mt), the sole unit of the low marginal belt group, is associated with the periphery of large tessera blocks of lower mean elevation and most commonly occurs along the contacts between the tessera and plains units. The unit has a mean elevation only about 0.7 km above the MPR.

Western (unit twf) and eastern (unit tef) Fortuna-type tesserae, Hina-type tessera (unit th), and intensely fractured tessera (unit tf) terrains are the highest tessera units of significant areal extent in the northern quarter of Venus, where they are associated primarily with Fortuna Tessera in Ishtar Terra. The mean elevations of these tessera units above the MPR range from a high of 3.53 km for the Hina-type tessera unit to a low of 1.53 km for the intensely fractured tessera terrain. The Laima-type tessera terrain (unit tl) and the tessera, undivided, terrain (unit tu) average only 0.64 km and 0.38 km above the MPR, respectively, and appear to have been regionally disrupted by tectonic and volcanic processes. These two units are commonly overlapped by units of the lowland plains group and mantled by the tessera-mantling plains unit (Schaber and Kozak, 1990). Such overlap and mantling is apparent in the regions south of Laima Tessera and north and east of Tellus Regio in the regions of Dekla, Meni, Ananke, and Kutue Tesserae (see U.S. Geological Survey, 1989).

Lineated terrain, type 1 (unit l_1) and lineated terrain, type 2 (unit l_2) have mean elevations 0.87 km and 0.54 km, respectively, below the MPR and -0.17 km and +0.16 km relative to the mean elevation of the smooth plains unit. Fractured terrain (unit f) has a mean elevation 0.75 km above the MPR and 1.45 km above the mean level of the smooth plains unit. The mean elevation of the ridge belt, type 1 terrain (unit rb_1) is close to that of lineated terrain, type 1 (unit l_1): 0.88 km below the MPR and 0.18 km below the mean elevation of the smooth plains unit. According to the merged Pioneer Venus and Venera 15/16 altimetric database used in this study, lineated terrain, type 1 and ridge belt, type 1 have the lowest mean elevations of the major terrain units mapped by Schaber and Kozak (1990). Three less extensive ridged terrains--the ridge complex (unit rc), ridge swarm (unit rs), and ridge belt, type 2 (unit rb_2)--have mean elevations at, 0.05 km below, and 0.52 km below the MPR, respectively.

Craters >45 km in diameter of suspected impact origin (unit c) and their probable ejecta deposits (unit ce) have mean elevations of 0.78 km and 0.51 km, respectively, below the MPR. The standard deviations in elevation of these crater units are only ±0.65 km and ±0.45 km, respectively.

The mean elevations and their standard deviations of the major terrain groups in the northern quarter of Venus illustrate well the overall hierarchy of terrains. The highland terrains are

dominated by the high marginal belt (6056.57±2.28 km) which averages 4.7 km above the MPR. The tessera group (6053.46±1.55 km) and the the upland plains group (6053.35±1.42 km) form a second elevation level at a mean of 1.5 km above the MPR. A third level with a mean elevation of about 6052 km is formed by the hilly terrain group, lower marginal belt group, shield/patera/tholus group, and domed upland group. The corona group (6051.88±0.62 km) forms a transitional fourth hypsometric level with a mean elevation exactly at the MPR, while the fifth and lowest elevation level at about 6051.3 km is made up of the lineated and fractured terrain group, the lowland plains group, the group of suspected impact craters >45 km in diameter, and the ridged terrain group. The mean elevation of this group actually lies 0.6 km below the MPR.

SURFACE PHYSICAL PROPERTIES

Scattering properties of part of surface of Venus were obtained by the Pioneer Venus and the Venera 15/16 spacecraft (Pettengill et al., 1980 1988; Abramov et al., 1989; Alexandrov et al., 1990). The parameters derived from the radar echos from these spacecraft included the C-parameter and rho, the power reflection coefficient (reflectivity) for normal incidence. The C-parameter corresponds to the inverse of the mean square, meter-scale surface slopes (in radians), or rms slope.

Data in a satisfactory digital and cartographic format were available to the author only from Pioneer Venus at the time of the preparation of this report. Values of rms slopes ($C\text{-power}^{-1/2}$) and the power reflection coefficient were acquired by Pioneer Venus only in the area between lat 60° S. and 75° N. (Pettengill et al., 1980). Thus, the terrain units mapped by Schaber and Kozak (1990) between 75° and 90° N. are not included in the following discussion of rms slope and reflectivity.

Rms Surface Slopes

Figure 18 and Table 3 give rms data for the included units; Figure 19 and Table 4, for the included groups.

The high marginal belt, low marginal belt, and tessera groups dominate the more rugged terrains, while the ridged terrain, lowland plains terrain, and lineated and fractured terrain groups form the most extensive surfaces with mean rms slopes between 2° and 3°.

Hina-type tessera and Lakshmi-type marginal belt terrains have the largest mean rms slopes and standard deviations of any unit mapped in the northern quarter of Venus (8.09°±4.00° and 7.45°±4.19°, respectively). (However, a single surface exposure of the Hina-type tessera unit in southern Fortuna Tessera covers only 0.23% of the map area.) Of the eight terrain units with the highest rms slopes, seven are tesserae with mean rms slopes between 4° and 8°.

The five ridged terrains have mean rms slopes between 2.3° and 3.0°, and thus they are intermediate between the rougher tesserae and the smoother lowland plains and lineated terrains. The

mapped part of the domed terrain of Bell Regio (unit bld) has a mean rms slope of 1.72°, which is even smoother than that of the smooth plains terrain. The tessera-mantling plains unit has a mean rms slope of 3.10°±2.38°; thus it is considerably rougher than the four plains units found at the lower elevations.

The corona, type 1 terrain (unit co_1) is characterized by circular or oblong sets of concentric ridges, while the corona, type 2 terrain (unit co_2) has smooth, annular ridges at Venera 15/16 image resolution (Schaber and Kozak, 1990); these differences in associated ridge roughness are reflected in the mean rms slopes computed for these units (3.48°±2.52° and 2.72°±1.04°, respectively).

The shield terrain (unit s) has a mean rms slope of 2.12°±0.89°, which is about the same as that of the smooth plains unit. Thus, any roughness associated with lava flow fields on the flanks of the shields is probably at a scale or slope-length too small to be determined from analyses of radar echoes returned from the nadir-viewing Pioneer Venus altimeter (Pettengill et al., 1980). The moderate incidence angles at which Magellan radar image data will be acquired will be better suited to sort out subtle differences in the small-scale roughness of lava flow fields.

The distribution of rms slopes for the 34 terrain units shows a general increase with elevation (Fig. 20; Table 3). A major exception however, is the smooth plains of Lakshmi Planum unit which is both relatively smooth (rms = 2.00°±0.77°) and about 3.6 km above the level of the lowland plains group.

Power Reflection Coefficient (Reflectivity)

Extremely weak radar echo returns and computed very low reflectivity values within parts of some tessera units (e.g., western and eastern Fortuna-type, intensely fractured, Laima-type, and undivided), the fractured terrain, and the tessera-type marginal belt units are considered to be misleading on the Pioneer Venus database used in this report. These values may result from excessive diffuse scattering of the radar echos from extremely rough terrains. Pettengill et al. (1988) used the imaging-mode data from Pioneer Venus to estimate the fraction of unmodeled, diffusely scattering surface between lat 20° S. and 50° N., and thus to correct the Pioneer Venus reflectivity values obtained from at least part of the map area. However, these data have not yet been merged and correlated with the terrain units mapped by Schaber and Kozak (1990) and the terrain groups described in this report.

Figure 21 and Table 3 give Pioneer Venus-derived reflectivity data for the included terrain units; Figure 22 and Table 4, for the included terrain groups.

The variations in the mean reflectivity computed for the 34 terrain units are relatively small, with a few exceptions. The Lakshmi-type marginal belt and Hina-type tessera units have reflectivities 2.2 and 1.6 times, respectively, higher than the

average (0.127) of the other 32 mapped units. This average value for the northern quarter of Venus is about the same as that (0.13±0.03) reported by Pettengill et al. (1980) for the the global mean reflection coefficient. Anomalously high reflection coefficients of 0.40±0.1 (Pettengill et al., 1988) to 0.60 (Alexandrov et al., 1990) for Maxwell Montes, and 0.40 and 0.45 for Akna and Freja Montes, respectively (Alexandrov et al., 1990) have strongly influenced the mean in reflectivity and standard deviation given here for the Lakshmi-type marginal belt unit. Such anomalies have been suggested to result from concentrations of some type of electrically conducting minerals (possibly sulfides or Fe/Ti oxides) embedded in the host rock (Pettengill et al., 1988). Jurgens et al. (1988) and Alexandrov et al. (1990) have suggested that high-reflectivity materials could be present on the surface and subsurface in the Venusian lowlands, as well as in the highland regions of anomalously high reflectivity reported by Pettengill et al. (1980, 1988).

Two large volcanic shields, Tepev and Sekmet Montes, have been described by Alexandrov et al. (1990) as possessing enhanced reflectivities of 0.35 and 0.40, respectively. In the present report, correlation of the Pioneer Venus reflectivity data with the shield unit indicates a mean value of 0.136±0.078, only 9% higher than the mean for the most pervasive plains unit, the smooth plains.

The craters of suspected impact origin >45 km in diameter (unit c) combined with their ejecta (unit ce) were found to have 11% higher mean reflectivity (0.138±0.080) than the smooth plains unit (0.127±0.077) but only 5% higher reflectivity than the lowland plains group (0.133±0.083).

The mean reflectivity and standard deviations for the 12 terrain groups illustrate the anomalous radar behavior of the high marginal belt group relative to the other terrain groups. The other groups have more consistent mean reflectivities, but their standard deviations differ significantly.

DISTRIBUTION OF SUSPECTED IMPACT CRATERS

Approximately 150 craters, whose morphologies are similar to those of impact craters elsewhere in the Solar System, were recognized by Ivanov et al. (1986) and Basilevsky et al. (1987) from Venera 15/16 data obtained between about lat 20° and 90° N. Schaber and Kozak (1990; plate 2) included 116 such structures, but they considered the remaining 34 to be of uncertain origin at the resolution of Venera 15/16 data. [Cleopatra Patera, a 100-km diameter crater located between 7.5 and 8.0 km above the MPR on the east flank of Maxwell Montes has been the subject of some controversy. This enigmatic feature has been interpreted from analysis of Venera 15/16, Pioneer Venus, and Earthbased radar data to have originated either through volcanic or volcano-tectonic processes (Masursky et al., 1980; Schaber et al., 1987a; Schaber and Kozak, 1990), or through impact-cratering processes (Ivanov et al., 1986; Basilevsky et al., 1987; Ivanov and Basilevsly, 1987; Ivanov, 1989; Basilevsky and Ivanov, 1990).

Magellan data should provide sufficient surface detail to confirm whether Cleopatra is indeed a volcanic patera, an impact basin, or possibly some combination of both. Cleopatra Patera has thus been intentionally left off the list of craters (Table 5) strongly suspected of being of impact origin based on pre-Magellan data].

The recognition of only 116 craters with impact-like morphology within a mapped area of 111.4 X 10^6 km^2 strongly suggests that the "average" surface of the northern quarter of Venus is much younger than the ancient surfaces of the Moon, Mars, and Mercury. Estimates as high as 1.0±0.5 b.y. have been suggested for the average age of that part of the northern quarter of Venus mapped by Venera 15/16; in making estimates workers have applied the lunar cratering rate averaged over the past 3.3 Ga (Ivanov et al., 1986; Basilevsky et al., 1987; Ivanov and Basilevsky, 1987). Assuming that the terrestrial cratering rate over the past 0.5 b.y. is more applicable to Venus, Schaber et al. (1987b) and Shoemaker and Shoemaker (in press) have suggested that the average surface in the northern quarter of Venus may be much younger than 1.0 Ga, perhaps a maximum of 450 m.y.---equivalent to the retention age estimated for the North American and European cratons on Earth.
Unfortunately, the small number of suspected impact craters >10 km in diameter within the northern quarter of Venus cannot support statistically confident determinations of crater size-frequency distributions and relative ages for individual terrain units or terrain groups. Arvidson et al. (1990), in addressing the nature and rate of resurfacing of Venus, favored a model in which crater-retention ages >>0.4 Ga possibly exist only for plains not subjected to recent volcanism or tectonism (governed by crater production and viscous relaxation); in their model are removed rapidy (>several km/Ga) by volcanism and tectonism. Significantly, their resurfacing model hat both volcanism and tectonism vary in magnitude over space and time.

What follows is a simple description of the correlations between actual numbers and densities of craters with elevation and mapped terrain units and terrain groups based on the available pre-Magellan crater data (Table 5). Statistical confirmation of the crater distributions and interpretations presented in this preliminary report must await the analyses of the complete Magellan dataset.

Longitudinal and Latitudinal Distribution

The longitudinal distribution of the craters (Fig. 23) appears to be rather uniform, except within two sectors. The sector between long 270° and 310° has slightly more craters than the longitudinal average, while the sector between long 177° and 270° appears to have slightly fewer. The first sector, immediately west of Lakshmi Planum, contains the maximum concentration of large coronae, while the second sector includes a large fan of ridge belts whose axis is centered along long 210° (Sukhanov and Pronin, 1987; Kozak and Schaber, 1989).

The latitudinal distribution of suspected impact craters between lat 25.9° and 87.2° N. has been computed for both 1° and 5° latitudinal bands (Figs. 24, 25). Eleven of the 1° latitudinal bands between lat 25° and 87° were not crossed by a crater; thus, the considerable deviations of the curve in figure 24 show no global trend. However, when the craters are placed in 5° latitudinal bins (Fig. 25), a strong trend of generally decreasing numbers of impact craters with decreasing latitude between 80° and 25° emerges. Regional deviations from that general trend can also be seen.

Crater Population and Density

Figure 26 shows the population of suspected impact craters recognized from Venera 15/16 data on the 22 cratered terrain units. Although the areally extensive smooth plains terrain has twice as many suspected impact craters as any other unit, a comparison of its areal coverage with its crater population shows its crater density to be only about half that of the other cratered terrains (Fig. 27). This discrepancy is also seen in the interpolated crater densities of the 22 cratered units (Fig. 28) and the deviations in crater density of 21 cratered units relative to the smooth plains unit (Fig. 29). On the basis of available data, we see that Lakshmi-type marginal belt terrain has the highest crater density, followed by the smooth plains of Lakshmi Planum terrain. The smooth plains unit has the fifth least cratered surface of the 22 cratered terrain units recognized. On the graph of crater densities of the 12 terrain groups (Fig. 30), the high marginal belts have the highest density-- more than 4 times that of the low plains group that contains the smooth plains. If Cleopatra Patera is shown by Magellan to be originally of impact origin, then the crater density of the high marginal belt unit (and group) is even greater relative to the other mapped units (and groups).

The reality and significance of these preliminary results--as yet statistically unsupportable--must await detailed scrutiny of the higher resolution Magellan data. A high-priority objective of the Magellan mission is to determine statistically valid crater size-frequency distributions from which at least relative surface ages can be determined for the different units. Knowledge of absolute surface ages will require reasonable estimates of the cratering rate at Venus over the past 500 million years or more.

Distribution in Elevation

The density of suspected impact craters on all cratered terrain units is plotted against elevation in Figure 31. No overall trends are apparent; however, a direct relation is clearly indicated for Lakshmi-type marginal belt terrain (unit ml) and the smooth plains of Lakshmi Planum (unit psl). [The western Fortuna-type tessera terrain (unit twf) is elevated but contains very few craters recognizable from the Venera 15/16 data]. A simple elevation plot of all 116 suspected impact

craters (Fig. 32) and a corrected plot (Fig. 33) show a clear separation of the same two groups. A more accurate portrayal of the densities of crater with elevation is revealed when these data are corrected for the percentage of the map area occurring at a given elevation (Fig. 17).

Crater Diameter and Elevation

A plot of crater diameter against elevation (Fig. 34) shows the same elevation clustering as in Figures 32 and 33. All of the craters between elevations of 6054 and 6056 km are less than 30 km in diameter, while 24 (23%) of the 106 craters found between 6050.5 and 6052.5 km are greater than 40 km in diameter. Six of those craters (6%) have diameters between 70 and 144 km.

ACKNOWLEDGMENTS

The author thanks Sherman Wu and Sherri Cantrell for digitization of the geologic/geomorphic map (Schaber and Kozak, 1990, Plate 1). Appreciation is also expressed to Eric Eliason, Nanci Isbell, Chris Isbell, and Tracie Stoewe for their help in digital processing of the map data and to John Chadwick for his support in analysis of impact crater data. Support to the U.S. Geological Survey was provided under Contract W15,415 from the NASA Planetary Geology and Geophysics Program, and under Contract WO 8,777 from the NASA Magellan Project Office.

REFERENCES CITED

Abramov, A.V., Grechischev, A.V., Zherihhin, N.V., Zheltikov, I.A., Kreslavsky, M.A., Levchenko, G.M., and Norozov, A.A., 1989, Scattering properties of Venus surface derived from Venera 15/16 data: (abstract). In Lunar and Planetary Science XX, Lunar and Planetary Institute, p. 3-4.

Alexandrov, Yu. N., Krivtsov, A.P., and Rzhiga, O.N., 1990, Venera 15 and 16 spacecraft: Some results of Venus surface reflectivity measurements: (abstract). In Lunar and Planetary Science XXI, Lunar and Planetary Institute, p. 13-14.

Arvidson, R.E., Grimm, R.E., Phillips, R.J., Schaber, G.G., and Shoemaker, E.M., 1990, On the nature and rate of resurfacing of Venus: Geophysical Research Letters, 19, 1385-1388.

Basilevsky, A.T., and Ivanov, B.A., 1990, Cleopatra crater on Venus: Venera 15/16 data and impact/volcanic origin controversy: Geophysical Research Lettters, 17, 175-178.

Basilevsky, A.T., Ivanov, B.A., Burba, G.A., Chernaya, I.M., Kryuchkov, V.P., Nikolaeva, O.V., Campbell, D.B., and Ronca, L.B., 1987, Impact craters of Venus: A continuation of the analysis of data from Venera 15 and 16 spacecraft: Journal of Geophysical Research, v. 92, p. 12,869-12,901.

Campbell, D.B., Head, J.W., Hine, A.A., Harmon, J.K., Senske, D.A., and Fisher, P.C., 1989, Styles of volcanism on Venus: New Arecibo high resolution radar data: Science, v. 246, p. 373-377.

Ford, P.G., 1986, Pioneer Venus hypsometry: Massachusetts

Institute of Technology Center for Space Research, Cambridge, Mass. 12 p.
Ivanov, B.A., 1989, Morphometry of impact craters on Venus [in Russian]: Astronomicheskii Vestnik, 23, 39-49, English translation in Solar System Research, 23, 23-31.
Ivanov, B.A. and Basilevsky, A.T., 1987, A comparison of crater retention ages on the Earth and Venus [in Russian]: Astronomicheskii Vestnik, 21, 136-143, English Translation in Solar System Research, 21, 84-88.
Ivanov,B.A., Basilevsky, A.T., Krychkov, V.P., and Chernaya, I.M., 1986, Impact craters of Venus: Analysis of Venera 15 and 16 data: Journal of Geophysical Research, v. 91, p. D413-D430.
Jurgens, R.F., Slade, M.A., and Saunders, R.S., 1988, Evidence for highly reflecting materials on the surface and subsurface of Venus: Science, v. 240, p. 1021-1023.
Kozak, R.C., and Schaber, G.G., 1989, New evidence for global tectonic zones on Venus: Geophysical Research Letters, v. 16, p. 175-178.
Masursky, Harold, Eliason, Eric, Ford, P.G., McGill, G.E., Pettengill, G.H., Schaber, G.G., and Schubert, Gerald, 1980, Pioneer Venus radar results: Geology from images and altimetry: Journal of Geophysical Research, v. 85, p. 8232-8260.
Pettengill, G.H., Eliason, E., Ford, P.G., Loriot, G.B., Masursky, Harold, and McGill, G.E., 1980, Pioneer Venus radar results: Altimetry and surface properties: Journal of Geophysical Research, v. 85, p. 8261-8270.
Pettengill, G.H., Ford, P.G., and Chapman, B.D., 1988, Venus: Surface electromagnetic properties: Journal of Geophysical Research, v. 93, p. 14,881-14,892.
Schaber, G.G., and Kozak, R.C., 1990, Geologic/geomorphic and structure maps of the northern quarter of Venus: U.S. Geological Survey Open-File Report 90-24, Denver, Colo., scale 1:15,000,000.
Schaber, G.G., Kozak, R.C., and Masursky, Harold, 1987a, Cleopatra Patera on Venus: Evidence for a volcanic origin: Geophysical Research Letters, v. 14, p. 41-44.
Schaber, G.G., Shoemaker, E.M., and Kozak, R.C., 1987b, The surface age of Venus: Use of the terrestrial cratering record [in Russian]: Astronomicheskii Vestnik, v. 21, p.144-151, English translation in Solar System Research, v. 21, p. 89-94.
Shoemaker, E.M. and Shoemaker, C.S., in press, Solar System roulette: The collision of solid bodies, in The new solar system: Cambridge, Mass., Sky Publishing.
Sukhanov, A.L., and Pronin, A.A., 1987, Evidence of tectonic spreading on Venus [in Russian]: Doklady Akademii Nauk SSSR, v. 294, p. 661-665; English translation in Transactions of the USSR Academy of Sciences, 1987, v. 294, p. 66-70.
Sukhanov, A.L., Pronin, A.A., Burba, G.A., Nikishin, A.M., Kryuchkov, V.P., Basilevsky, A.T., Markov, M.S., Kuzmin,

R.O., Bobina, N.N., Shashkina, V.P., Slyuta, E.N., and Chernaya, I.M., 1989, Geomorphic/geologic map of part of the northern hemisphere of Venus: U.S. Geological Survey Miscellaneous Investigations Series Map I-2059, scale 1:15,000,000.

U.S. Geological Survey, 1989, Maps of part of the northern hemisphere of Venus: U.S. Geological Survey Miscellaneous Investigations Series Map I-2041, 3 sheets, scale 1:15,000,000.

FIGURE CAPTIONS

[In Figures 1-12, latitude bounding data at long 0° is 28.3° N.; at long 90° it is 27.7° N.; at long 180° it is 46.5° N.; and at long 270° it is 31.5° N.]

Figure 1a - Distribution of lowland plains terrain group. Group consists of the following geologic/geomorphic terrain units: smooth plains, intermediate plains, mottled plains, complex plains, and domical hill or hill field.

Figure 1b - Distribution of smooth plains terrain unit

Figure 2 - Distribution of lineated and fractured terrain group, consisting of lineated terrain, type 1;, lineated terrain, type 2; fractured terrain; and ridge complex terrain.

Figure 3 - Distribution of tessera terrain group, consisting of Laima-type tessera; western Fortuna-type tessera; eastern Fortuna-type tessera; Hina-type tessera; intensely fractured tessera; and tessera, undivided, units.

Figure 4 - Distribution of ridged plains group, consisting of ridge; ridge belt, type 1; ridge belt, type 2; and ridge swarm units.

Figure 5 - Distribution of upland plains terrain group, consisting of smooth plains of Lakshmi Planum and tessera-mantling plains units.

Figure 6 - Distribution of shield/patera/tholus terrain group, consisting of shield, crater (patera), and domical mesa (tholus) units.

Figure 7 - Distribution of domed upland terrain group, consisting of domed terrain of Beta Regio and domed terrain of Bell Regio.

Figure 8 - Distribution of corona terrain group, consisting of corona, type 1, and corona, type 2, units.

Figure 9 - Distribution of low marginal belt terrain group. Contains only tessera-type marginal belt unit.

Figure 10 - Distribution of high marginal belt terrain group. Group contains only Lakshmi-type marginal belt unit.

Figure 11 - Distribution of hilly terrain group. Group contains only hilly terrain unit.

Figure 12 - Distribution of terrain group containing suspected impact craters >45 km in diameter and their ejecta.

Figure 13 - Percentages of map area covered by each of the 34 terrain units. See Table 1 for explanation of symbols.

Figure 14 - Percentage of map area covered by each of the 12 terrain groups. See Table 2 for explanation of symbols and included terrain units.

Figure 15 - Mean elevations and standard deviations of the 34 terrain units. See Table 1 for explanation of symbols. High and low elevation bars represent the standard error, not absolute elevations.

Figure 16 - Mean elevations and standard deviations of the 12 terrain groups. See Fig. 15 for explanation of high and low elevation bars.

Figure 17 - Percentages of the region mapped by Schaber and Kozak (1990) at various elevations.

Figure 18 - Mean rms slopes and standard deviations for the 34 terrain units between about lat 25° N. and 75° N. See Table 1 for explanation of symbols. See Fig. 15 for explanation of high and low elevation bars.

Figure 19 - Mean rms slopes and standard deviations for the 12 terrain groups between about lat 25°N. and 75° N. See Table 2 for explanation of symbols. See Fig. 15 for explanation of high and low elevation bars.

Figure 20 - Relation between rms slope and elevation for the 34 terrain units between about lat 25° N. and 75° N. See Table 1 for explanation of symbols.

Figure 21 - Mean reflectivities and standard deviations for the 34 terrain units between about lat 25° N. and 75° N. See Table 1 for explanation of symbols. See Fig. 15 for explanation of high and low elevation bars.

Figure 22 - Mean reflectivities and standard deviations for the 12 terrain groups between about lat 25° and 75° N. See Table 2 for explanation of symbols. See Fig. 15 for explanation of high and low elevation bars.

Figure 23 - Longitudinal distribution of 116 suspected impact craters >10 km in diameter within the area mapped by Schaber and Kozak (1990).

Figure 24 - Relative abundance of suspected impact craters >10 km in diameter in 1° latitudinal bins. Decrease in circumference of latitude bands with increasing latitude was taken into consideration by arbitrarily assigning a value of 1 to the highest latitude band containing a crater (87.2° N.), to which all other latitudinal bands were normalized.

Figure 25 - Relative abundance of suspected impact craters >10 km in diameter in 5° latitudinal bins. Bands normalized as described in figure 24.

Figure 26 - Number of suspected impact craters >10 km in diameter recognized on 22 terrain units. Remaining 12 units mapped had no recognizable impact craters. See Table 1 for explanation of symbols.

Figure 27 - Relation between population of impact craters >10 km in diameter recognized on 22 terrain units and percentage of map area covered by those units. Combined populations of intermediate (unit pi), mottled (unit pm), and complex (unit pc) fall at top center. See Table 1 for explanation of other symbols.

Figure 28 - Density of suspected impact craters >10 km in diameter per 1,000,000 km^2 for each of the 22 cratered terrain units. See Table 1 for explanation of symbols.

Figure 29 - Deviations in density of suspected impact craters >10 km in diameter for 21 cratered terrain units relative to that of smooth plains unit, which has a value of 0 on the y axis. See Table 1 for explanation of symbols.

Figure 30 - Density of suspected impact craters >10 km in diameter for nine terrain groups. No impact craters were recognized on the remaining terrain groups. See Table 2 for explanation of symbols.

Figure 31 - Relation between density of suspected impact craters >10 km in diameter on the 22 cratered terrain units and mean elevation of those units. See Table 1 for explanation of symbols.

Figure 32 - Elevation of 116 craters >10 km in diameter of suspected impact origin within map area. Note clustering of craters into two elevation groups.

Figure 33 - Density of suspected impact craters relative to area-

corrected elevation. Elevations were normalized by using the hypsometric data shown in figure 15. Elevation data plotted in 0.5-km bins.

Figure 34 - Relation between diameter and elevation of 116 suspected impact craters within map area. Crater diameters taken from Basilevsky et al. (1987). Crater names for some of the highest and largest craters are given for convenience. Cleopatra is queried because of the controversy concerning its impact or volcanic origin (Ivanov et al., 1986; Basilevsky et al., 1987; Schaber et al., 1987).

Table 1 - Terrain units mapped by Schaber and Kozak (1990)
(in order of decreasing abundance)

Symbol	Unit Name
ps	Smooth Plains
pi	Intermediate Plains
l1	Lineated Terrain, Type 1
l2	Lineated Terrain, Type 2
rb1	Ridge Belt, Type 1
pm	Mottled Plains
pt	Tessera-Mantling Plains
tl	Laima-Type Tessera
dh	Domical Hill or Hill Field
pc	Complex Plains
tu	Tessera, Undivided
rs	Ridge Swarm
s	Shield
twf	Western Fortuna-Type Tessera
rc	Ridge Complex
f	Fractured Terrain
mt	Tessera-Type Marginal Belt
col	Corona, Type 1
bld	Domed Terrain of Bell Regio
tef	Eastern Fortuna-Type Tessera
cp	Crater (Patera)
psl	Smooth Plains of Lakshmi Planum
btd	Domed Terrain of Beta Regio
ml	Lakshmi-Type Marginal Belt
rb2	Ridge Belt, Type 2
tf	Fractured Tessera
co2	Corona, Type 2
r	Ridge
h	Hilly Terrain
th	Hina-Type Tessera
ce	Ejecta of Suspected Impact Crater
c	Suspected Impact Crater
dm	Domical Mesa (Tholus)
tg	Grooved Tessera

Table 2 - Terrain groups described in this report (in order of decreasing abundance)

Symbol	Group	Terrain Units Included (See Table 1 for explanation of symbols)
LP	Lowland Plains	ps,pi,pm,pc,dh
LFT	Lineated & Fractured Terrain	l1,l2,f,rc
T	Tessera	tl,twf,tef,th,tg,tf,tu
RT	Ridged Terrain	r,rb1,rb2,rs
UP	Upland Plains	psl,pt
SPT	Shield/Patera/Tholus	s,cp,dm
DU	Domed Uplands	btd,bld
CO	Corona	co1,co2
LMB	Low Marginal Belt	mt
HMB	High Marginal Belt	ml
HT	Hilly Terrain	ht
CRT>45km	Suspected Impact Crts>45 km	c,ce

Table 3 - Physical Parameters and Impact Crater Densities of the 34 Terrain Units Mapped by Schaber and Kozak (1990).

Unit Symbol	Area (10^6 km^2)	% of map area	Mean elev. (km)	SD in elev. (km)	Mean rms slope (°)	SD in rms slope (°)	Mean refl.	SD in refl.	Number of impact crts.	Impact crts/ 10^6 km^2
ps	36.79	33.03	6051.20	0.54	2.17	0.80	0.127	0.077	26	0.71
pi	9.48	8.51	6051.35	0.67	2.27	1.17	0.132	0.082	13	1.37
l1	7.03	6.32	6051.03	0.56	1.78	0.77	0.152	0.085	13	1.85
l2	6.75	6.06	6051.36	0.67	2.11	0.91	0.143	0.083	12	1.78
rb1	6.08	5.46	6051.02	0.70	3.06	1.53	0.112	0.086	5	0.82
pm	5.47	4.91	6051.84	0.54	2.20	1.02	0.155	0.095	6	1.10
pt	4.40	3.96	6053.01	1.60	3.10	2.38	0.129	0.127	7	1.59
tl	3.79	3.40	6052.54	0.70	4.24	2.60	0.044	0.116	2	0.53
dh	3.72	3.34	6051.55	0.47	2.27	0.83	0.137	0.081	4	1.07
pc	3.10	2.78	6051.13	0.50	2.21	0.92	0.146	0.093	6	1.94
tu	3.06	2.75	6052.28	1.00	3.94	2.48	0.122	0.126	4	1.31
rs	3.06	2.75	6051.46	0.58	2.29	0.92	0.125	0.074	2	0.65
s	2.99	2.69	6052.65	1.24	2.12	0.89	0.136	0.078	3	1.00
twf	2.00	1.79	6054.99	1.52	5.43	3.24	0.151	0.163	1	0.50
rc	1.48	1.33	6051.85	0.59	2.92	1.43	0.127	0.091	1	0.68
f	1.37	1.23	6052.65	1.51	3.07	2.06	0.132	0.122	0	----
mt	1.30	1.17	6052.57	1.15	4.72	3.30	0.126	0.132	1	0.77
col	1.19	1.07	6051.98	0.59	3.48	2.52	0.139	0.111	0	----
bld	1.18	1.06	6051.91	0.68	1.72	0.91	0.116	0.067	2	1.69
tef	1.06	0.96	6053.52	0.76	5.57	3.48	0.118	0.122	1	0.94
cp	0.95	0.86	6051.94	1.16	2.61	1.10	0.129	0.090	0	----
ps1	0.93	0.83	6054.94	0.57	2.00	0.77	0.132	0.082	2	2.16
btd	0.76	0.68	6053.40	1.06	3.68	1.77	0.112	0.083	0	----
ml	0.76	0.68	6056.57	2.28	7.45	4.19	0.275	0.227	3	3.96
rb2	0.59	0.53	6051.38	0.54	3.01	1.95	0.123	0.087	1	1.70
tf	0.52	0.47	6053.43	1.01	4.52	2.85	0.128	0.134	1	1.90
co2	0.41	0.37	6051.38	0.47	2.72	1.04	0.112	0.068	0	----
r	0.34	0.30	6051.24	0.66	2.57	1.19	0.134	0.081	0	----
h	0.26	0.23	6052.74	0.82	3.35	1.58	0.127	0.078	0	----
th	0.25	0.23	6055.32	0.67	8.09	4.00	0.207	0.189	0	----
ce	0.13	0.12	6051.39	0.45	1.79	0.67	0.134	0.075	0	----
c	0.07	0.06	6051.12	0.65	1.98	1.10	0.147	0.088	0	----
dm	0.05	0.05	6051.45	0.52	2.20	1.05	0.114	0.071	0	----
tg	0.04	0.04	6055.51	0.12	2.31	0.43	0.104	0.054	0	----

Table 4 - Physical Parameters and Impact Crater Densities for the 12 Terrain Groups Described in this Report.

Group Symbol	Area (10^6 km^2)	% of map area	Elevation (km)	SD in Elev. (km)	Mean rms slope (°)	SD in rms slope (°)	Mean refl.	SD in refl.	Number of impact crts.	Impact crts/ 10^6 km^2
LP	52.58	58.57	6051.30	0.59	2.20	0.90	0.133	0.083	55	0.94
LFT	14.94	16.63	6051.36	0.82	2.14	1.15	0.144	0.089	26	1.56
T	9.64	10.72	6053.46	1.55	4.82	3.09	0.127	0.141	9	0.84
RT	9.05	10.07	6051.14	0.70	2.79	1.43	0.118	0.083	8	0.79
UP	4.79	5.33	6053.35	1.42	2.91	2.10	0.130	0.119	9	1.69
SPT	3.60	3.99	6052.50	1.26	2.22	0.95	0.135	0.080	3	0.75
DU	1.74	1.94	6052.49	1.12	3.05	1.80	0.114	0.079	2	1.94
CO	1.44	1.60	6051.88	0.62	3.33	2.32	0.134	0.106	0	0
LMB	1.17	1.30	6052.57	1.15	4.72	3.30	0.126	0.132	1	0.77
HMB	0.68	0.76	6056.57	2.28	7.45	4.19	0.275	0.227	3	3.96
HT	0.23	0.26	6052.74	0.82	3.35	1.58	0.127	0.078	0	0
CR>45 KM	0.18	0.20	6051.29	0.55	1.85	0.84	0.138	0.080	0	0

Table 5 - Suspected Impact Craters >10 km in Diameter
Between lat 25° N. and 90° N. (in order of decreasing latitude)

Terrain Unit	Latitude (°)	Longitude (°)	Elevation (km)	Crater Name	Diameter (km)
ps	87.2	290.5	6050.67	UNNAMED	
pc	85.35	214.5	6051.30	TATYANA	22
pi	84.6	79	6050.20	LANDOWSKA	38
pc	84.05	16.5	6050.49	RUSLANOVA	44
pc	82.55	273.5	6051.40	UNNAMED	26
rb1	81.35	200	6051.85	UNNAMED	--
pc	81.15	285.5	6051.51	LAGERLOF	58
pi	81.05	223.5	6051.62	EFIMOVA	30
dh	78.45	173.9	6051.78	RUDNEVA	34
tef	78.25	306.5	6052.82	DSAHKOVA	50
rb1	78.1	76.5	6050.70	GINA	22
dh	76.9	192.5	6052.11	TUNDE	16
twf	76.25	17	6054.44	FERNANDEZ	27
l1	76.2	104.5	6051.29	KLENOVA	144
pi	75.95	55.5	6051.47	ULRIQUE	22
l1	75.8	127	6051.40	DELEDDA	32
l1	75.55	96	6051.54	RADKA	15
pi	75.5	272	6051.99	VALBORG	20
rb2	74.7	176.6	6051.85	DICKINSON	72
l2	72.25	121.5	6051.85	MONIKA	30
ps	72.1	174.8	6051.65	ERIKA	14
ml	71.2	322.75	6055.16	WANDA	22
psl	70.9	335.25	6055.20	RITA	11
rc	70.7	300	6052.65	COTTON	52
ml	70.65	320.5	6055.80	OSIPENKO	32
pt	70.5	289.75	6051.99	OBUKHOVA	44
pm	70.1	107.25	6051.61	LAFAYETTE	46
rb1	69.25	236.25	6051.52	ZOYA	22
pm	68.45	94.2	6052.33	GLORIA	23
pm	68.4	90.5	6052.07	JADWIGA	15
pt	68.2	303.75	6052.31	IVKA	18
l2	68	292	6051.32	DUNCAN	46
s	67.1	273	6051.96	NATALIA	12
tu	67.05	329.5	6055.32	MAGDA	16
l1	65.45	168.75	6050.15	UNNAMED	34
pt	65.1	299	6051.64	ZDRAVKA	14
vs	64.6	334.5	6054.78	ZLATA	10
pm	64.4	139.5	6051.90	KOIDULA	72
l1	64.2	159.5	6050.02	UNNAMED	--
l1	64.1	289.75	6050.83	INDIRA	16
pt	63.45	314.5	6053.63	SIGRID	21
pi	62.85	88	6051.69	MASHA	21
vs	62.15	329.75	6054.42	LYUDMILA	20
psl	62.1	321.75	6054.23	BERTA	28
ml	61.55	317.5	6054.36	TAMARA	10
pt	61.35	308	6051.58	AKHMATOVA	44
ps	61.3	223	6051.39	BARSOVA	80
pc	60.4	154.5	6050.40	EMOLOVA	66
pi	60.3	286.5	6051.00	GOLUBKINA	28
l2	60	272.9	6051.27	MARGIT	16
rs	59.8	65.6	6051.37	FEDORETS	52
l2	59.3	279.7	6051.02	MONTESORI	44
tu	58.3	336.9	6053.79	MAGNANI	28
pt	56.9	6.5	6054.86	ROSSETTI	24

Table 5 - Continued

tu	56.5	235.1	6051.71	ORLOVA	26
tu	56.4	242.5	6051.74	UNNAMED	16
mt	55.7	61.9	6051.57	WHARTON	54
l2	53.9	243.8	6051.38	HAYASI	44
ps	52.45	326.2	6050.76	UNNAMED	32
pm	51.9	143.4	6051.11	COCHRAN	104
pi	51.9	254.5	6051.58	UNNAMED	28
l2	51.8	201.6	6051.64	DOLORES	16
ps	51.75	291.7	6050.54	OLYA	17
pi	51.7	60.55	6051.66	UNSET	33
pi	51.3	333.2	6051.33	STEPHANIA	15
pi	51.15	335.7	6051.34	LOTTA	16
ps	51.05	242.5	6051.55	JULIE	16
ps	50.25	354.9	6051.75	LIND	28
pc	49.9	75.1	6051.54	NANA	15
l2	48.45	140.8	6051.55	LAURA	19
rbl	48.4	296.6	6050.51	BROOKE	24
l1	48.3	195.3	6051.33	YBLOCHKNA	58
ps	47.8	307.1	6050.61	GALINA	20
pm	47.8	14.7	6052.08	KEMBLE	24
ps	47.2	106.8	6051.54	CATHER	29
pi	46.8	123	6051.76	ALMEIDA	19
l2	46.6	143.9	6051.41	VALENTINA	26
l2	45.5	146.3	6051.04	BARTO	50
ps	45.5	281.6	6050.57	UNNAMED	19
l1	45.45	171.6	6050.32	FEDOSOVA	56
ps	45.35	283	6050.58	ZVEREVA	24
tl	45.35	49.7	6051.32	UNNAMED	--
ps	45	254.5	6051.01	UNNAMED	--
ps	44.9	32.4	6051.92	UNNAMED	--
rs	44.45	201.4	6050.95	NADIRA	34
l1	44.2	11.4	6051.49	PRICHARD	24
ps	44.1	359.8	6051.23	ARIADNE	27
l1	43.4	19.8	6051.67	RUTH	20
ps	42.55	148.05	6051.22	POLINA	22
dh	41.95	320	6050.72	ZINA	12
dh	41.8	122.3	6051.25	TAGLIONI	32
ps	40.55	149.25	6051.11	UNNAMED	--
ps	40.1	331.4	6050.92	JEANNE	22
ps	39.5	297.7	6051.15	ANYA	21
l1	39.4	22.75	6051.17	LENA	16
ps	38.7	292.1	6051.27	UNNAMED	19
l1	37.95	41.5	6051.21	UNNAMED	32
l2	37.65	22.7	6051.46	STINA	12
pt	36.6	274	6052.43	UNNAMED	--
l1	36.25	31.8	6051.21	UNNAMED	25
bld	35.7	56	6051.29	VOYNICH	56
rbl	35	301.5	6051.88	UNNAMED	--
ps	34.95	91	6051.46	IRINA	18
ps	34.6	119.8	6051.22	MOSES	30
l2	33.75	22.65	6051.61	UNNAMED	20
tl	32.7	84.4	6052.72	BERNHARDT	28
l2	32.3	22.6	6051.70	EDGEWORTH	32
bld	31.75	53	6051.69	POTANINA	96
ps	30.2	31	6051.76	LILLYA	20
ps	30	147.2	6051.28	REGINA	26
ps	29.65	0.4	6051.73	MUKHINA	28
tf	28.6	79.2	6051.82	TSERSKAYA	36

Table 5 - Continued

ps	28.4	4.7	6051.30	BROWNING	26
ps	28.2	106.8	6050.52	ANTONINA	17
pi	28.1	72.65	6050.92	CHRISTIE	28
pi	25.9	72.7	6050.62	UNNAMED	57

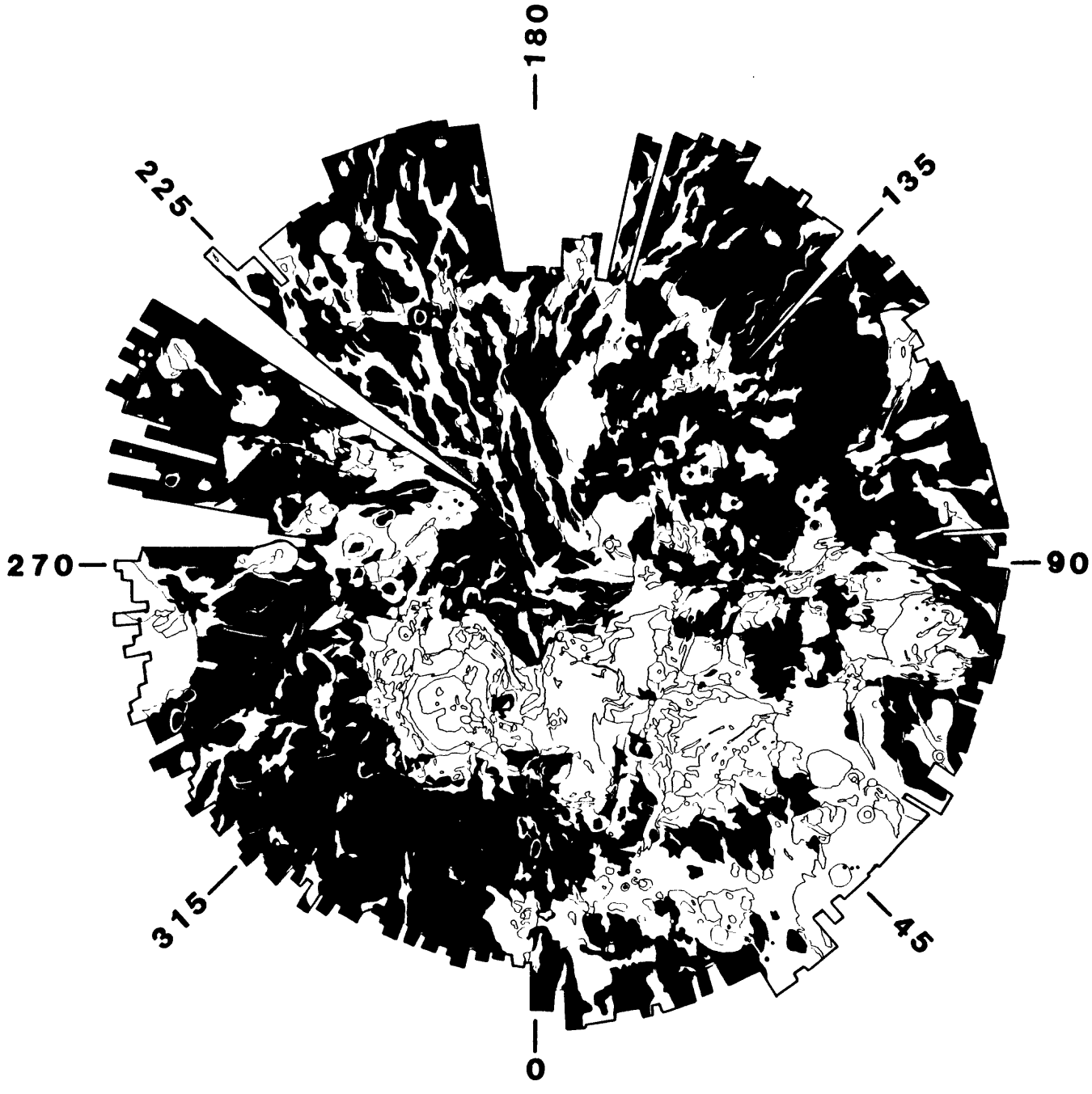

Fig. 1a

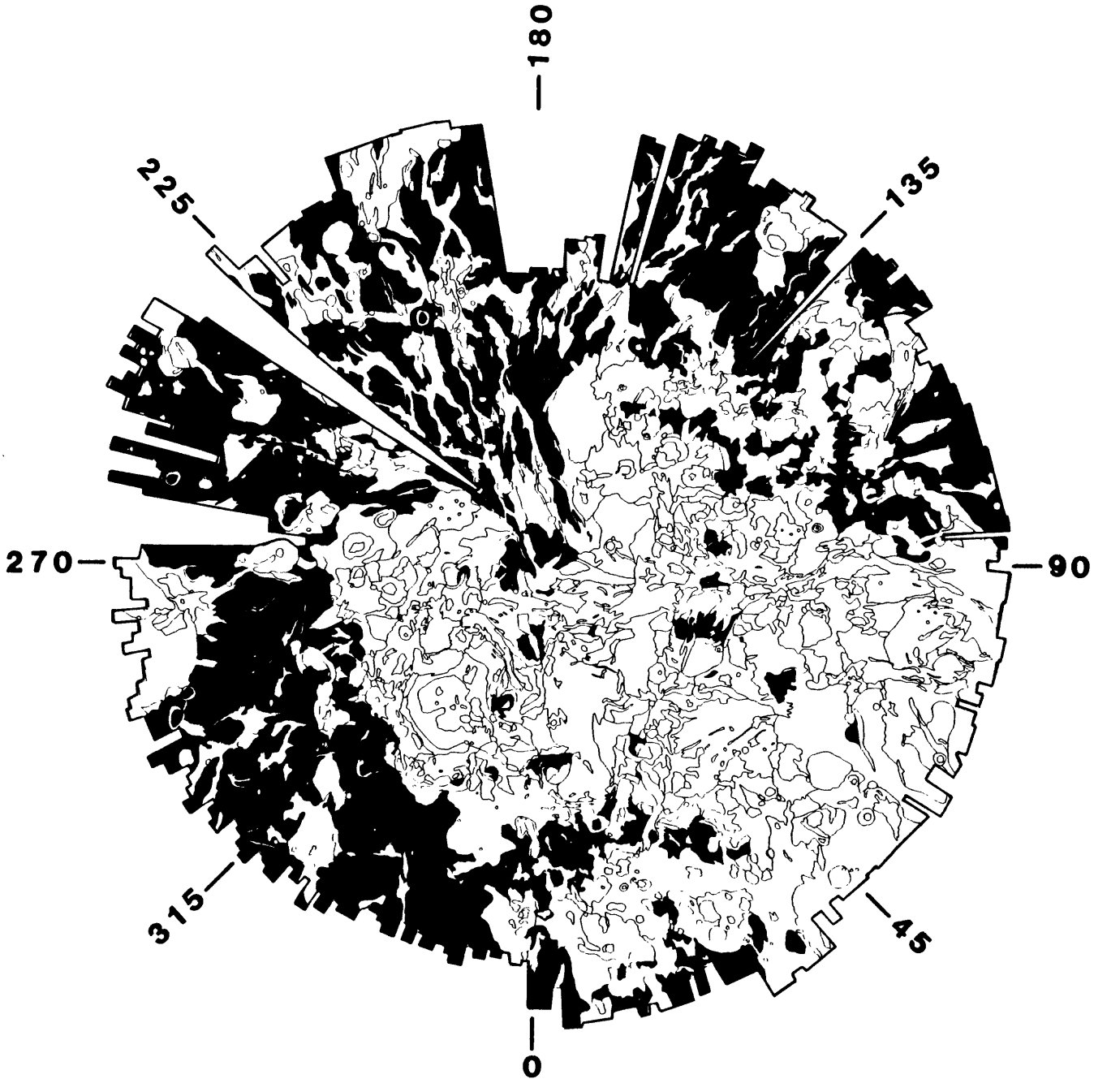

Fig. 1b

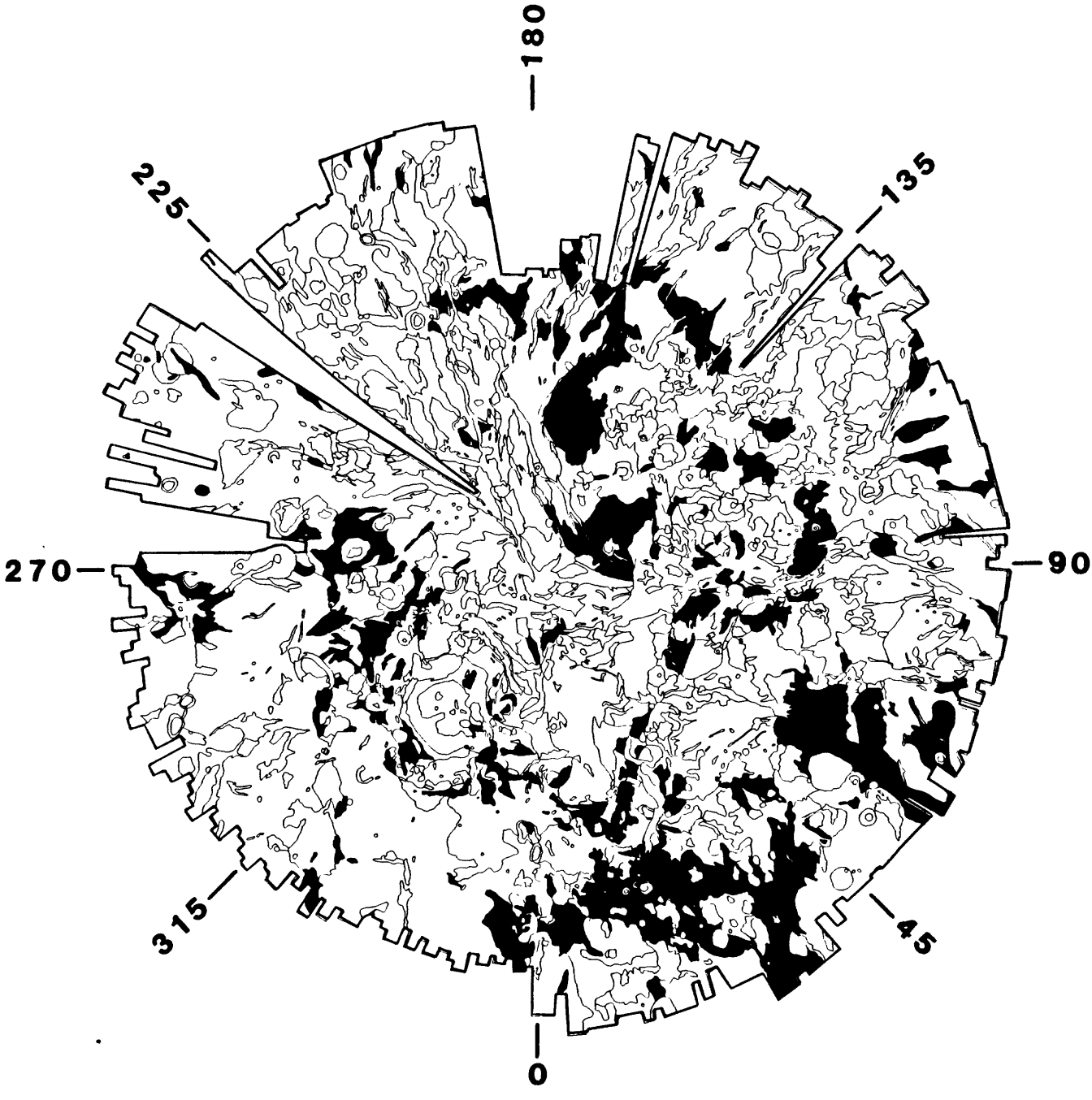

Fig. 2

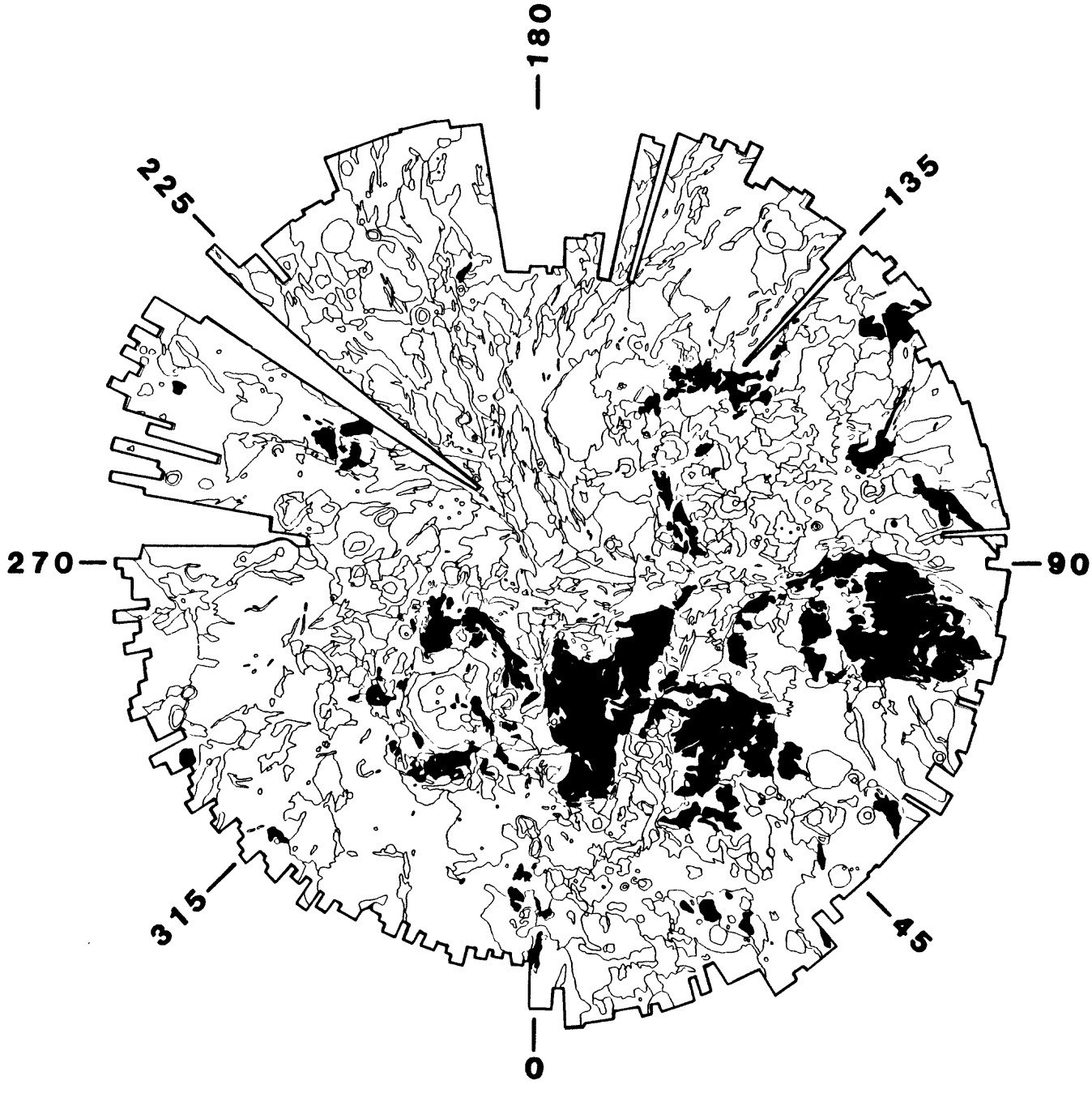

Fig. 3

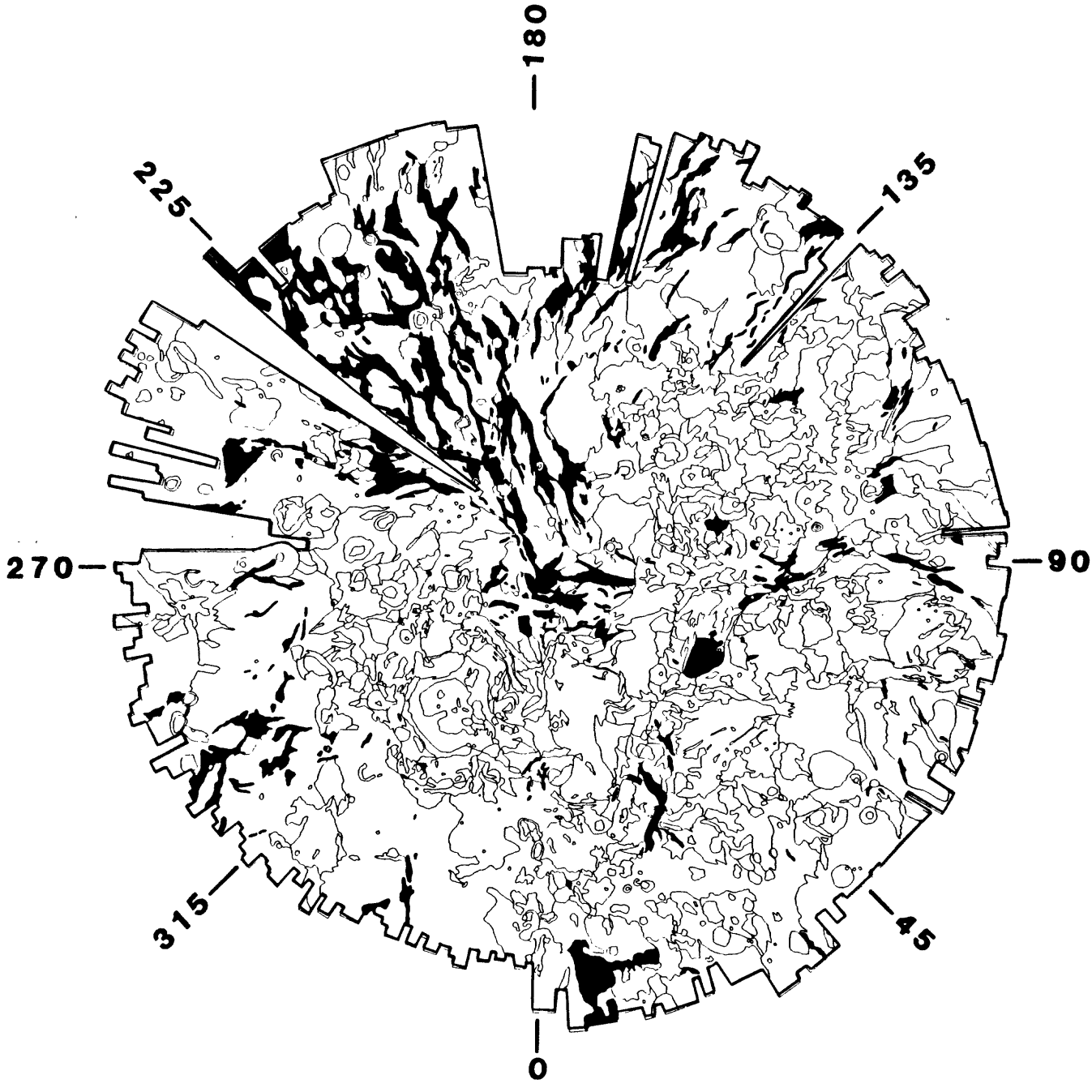

Fig. 4

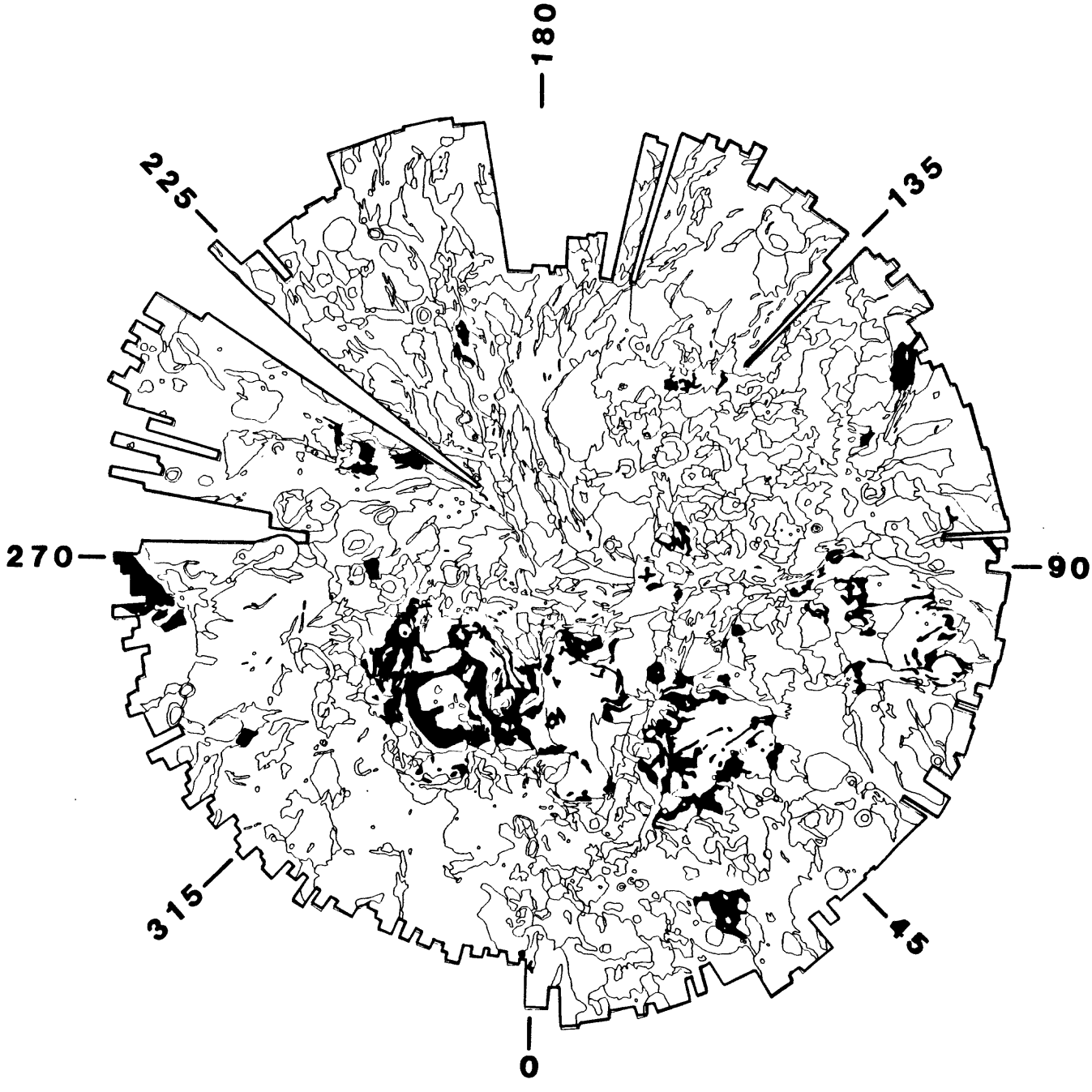

Fig. 5

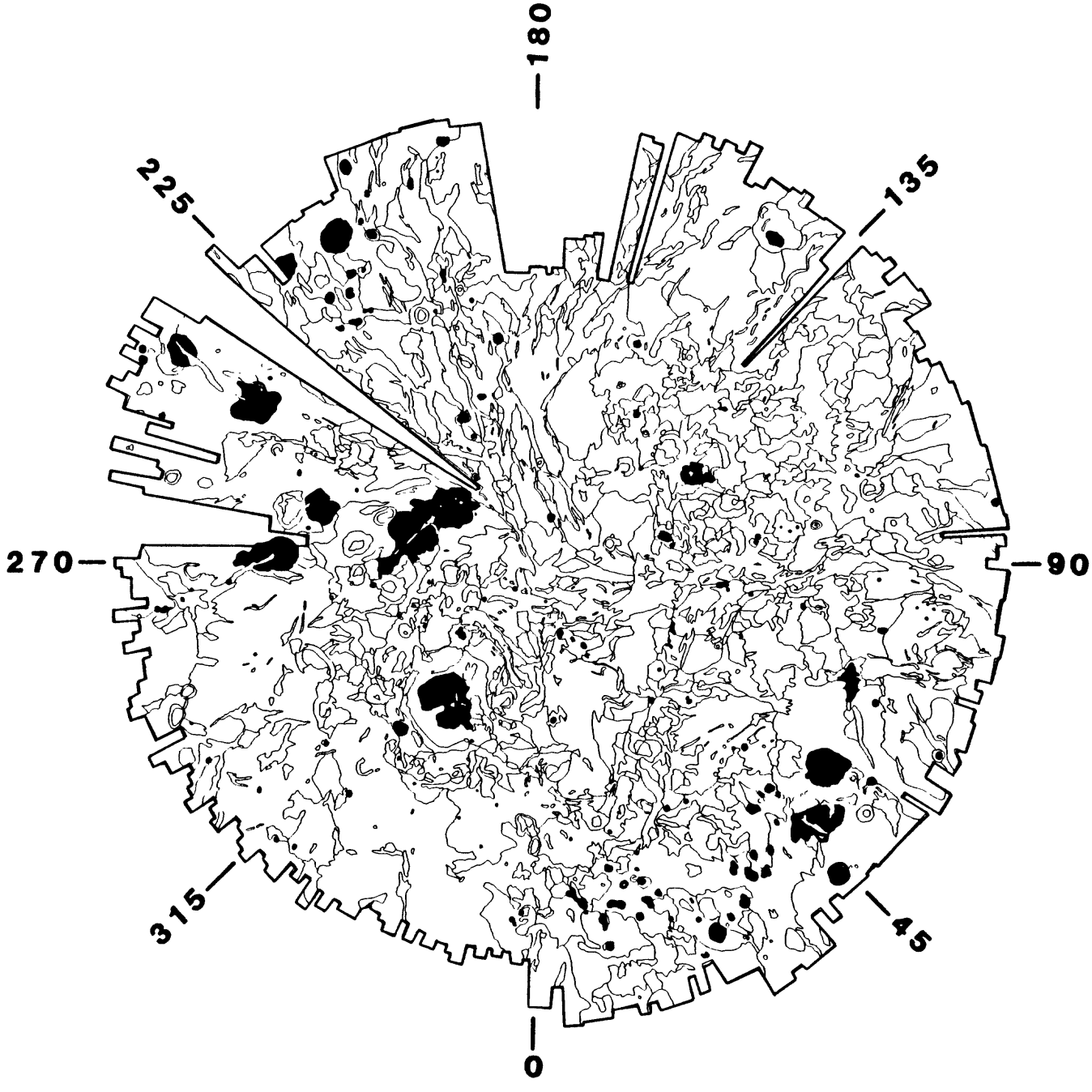

Fig. 6

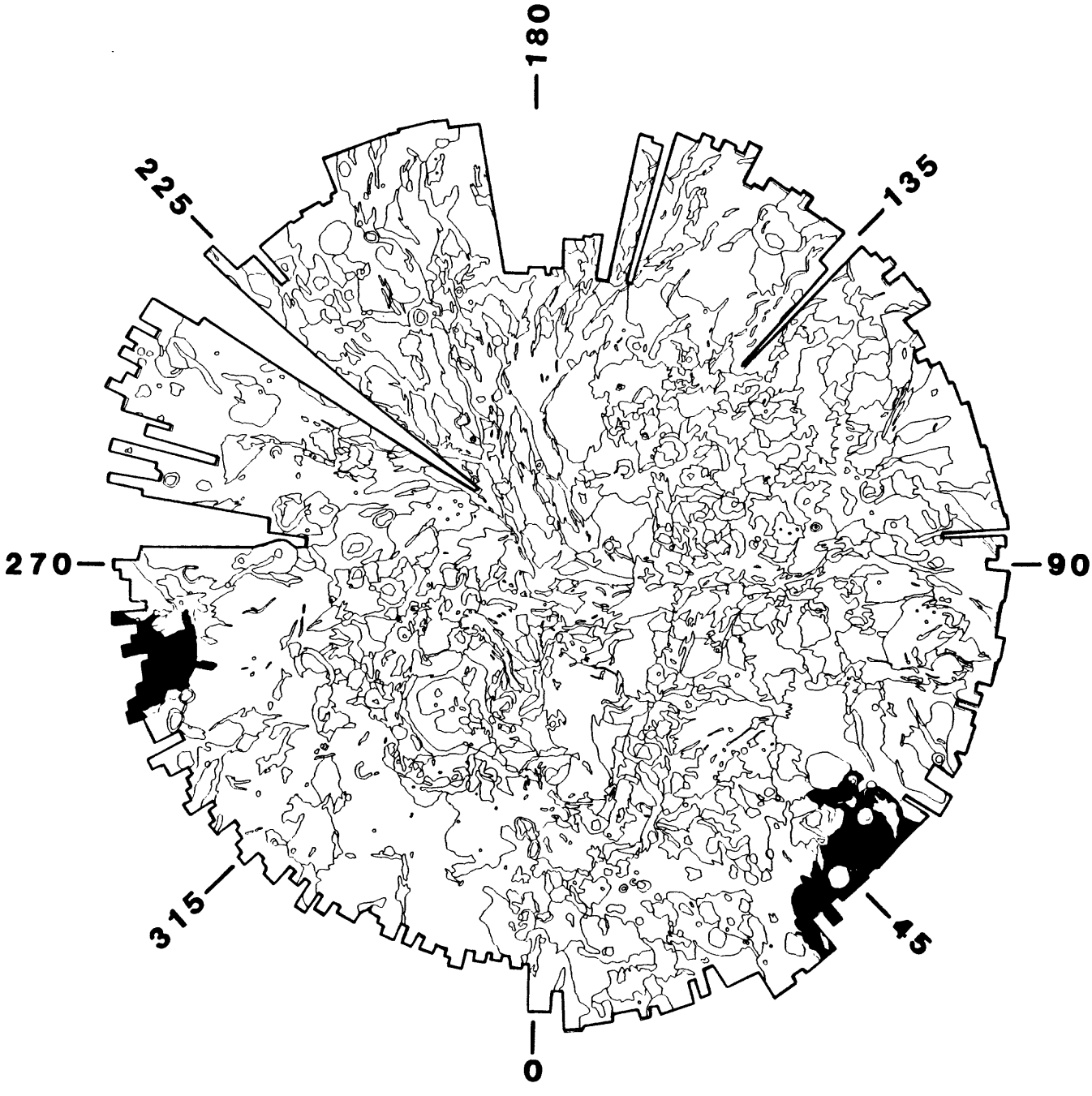

Fig. 7

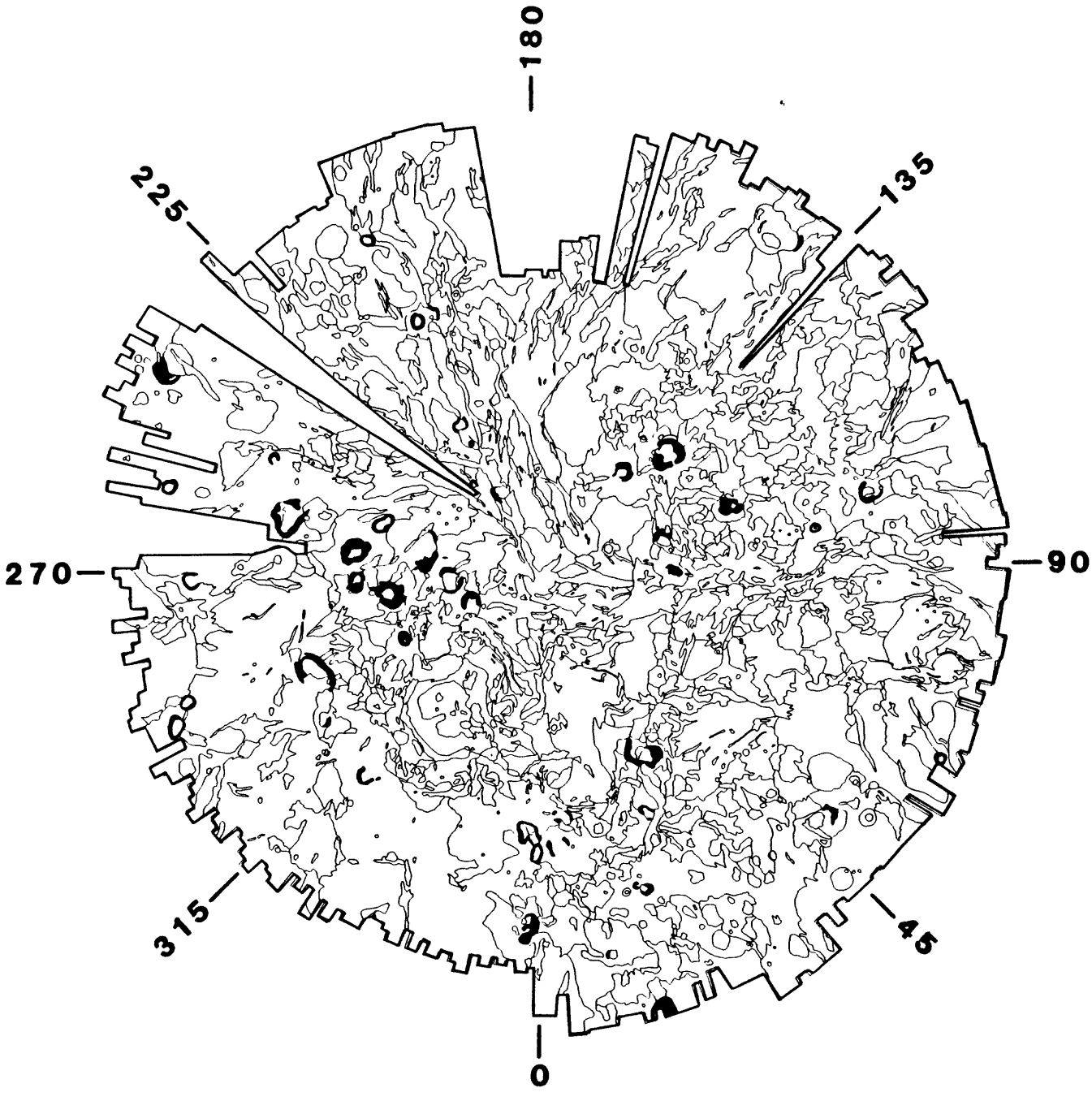

Fig. 8

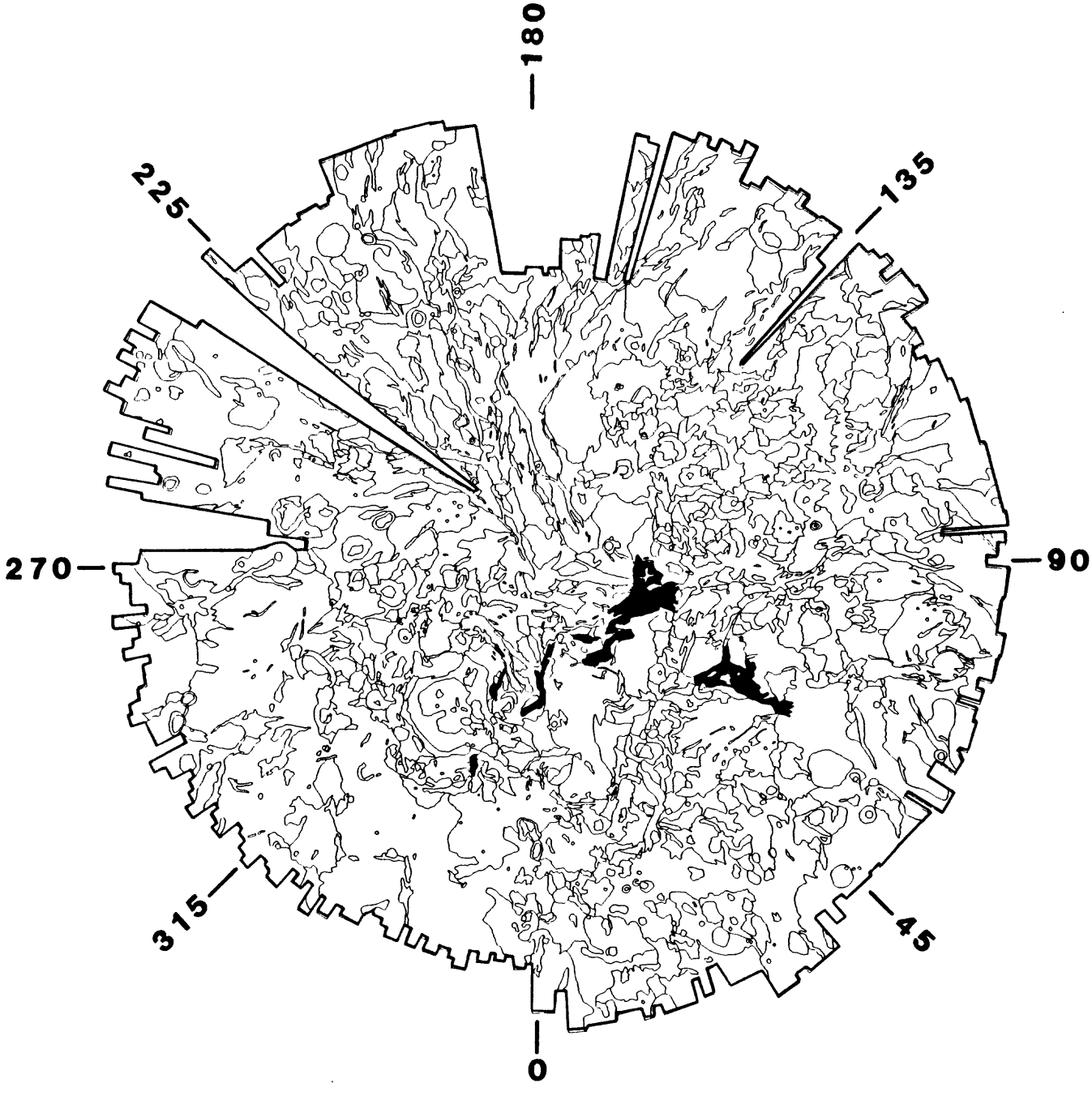

Fig. 9

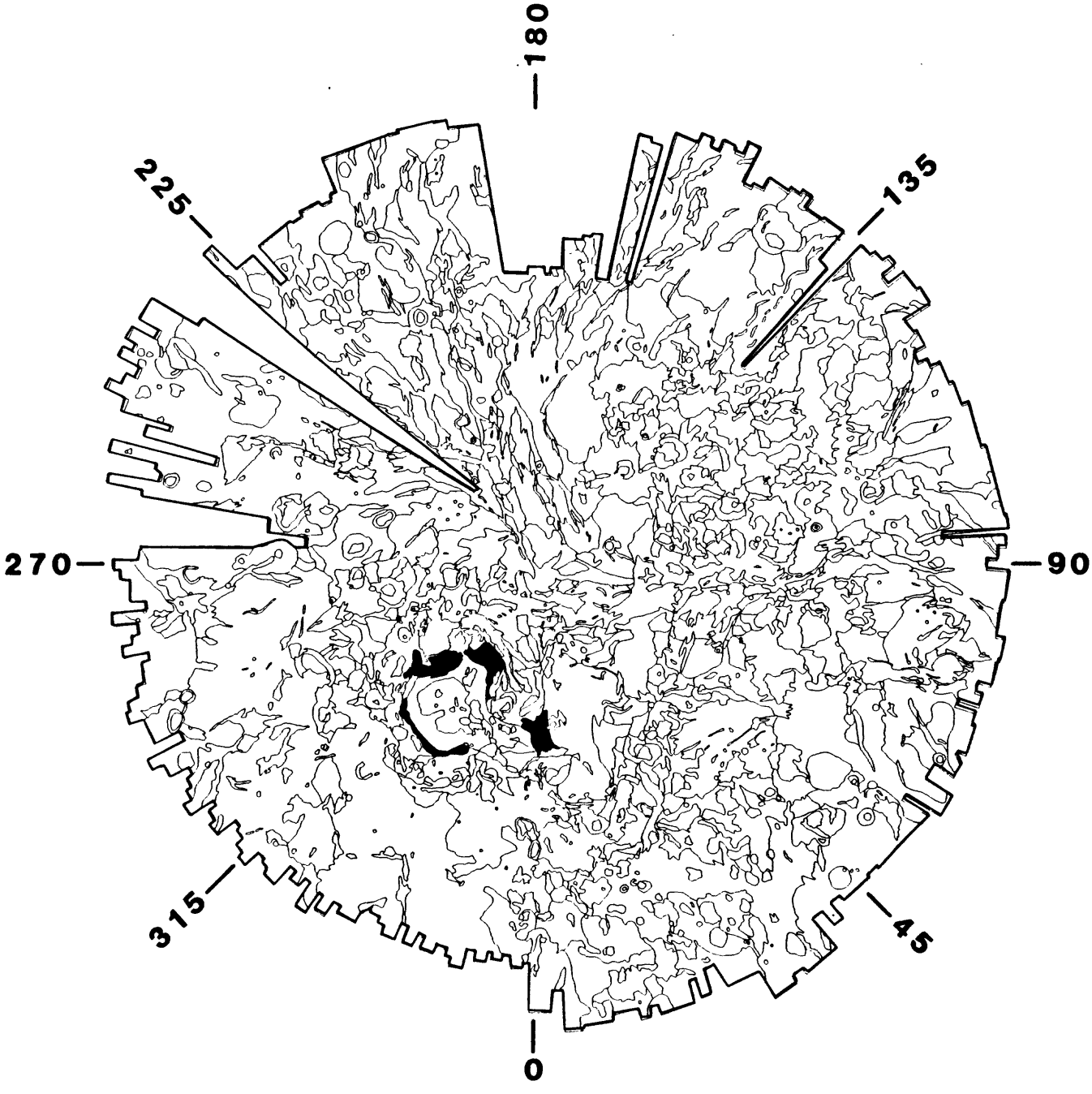

Fig. 10

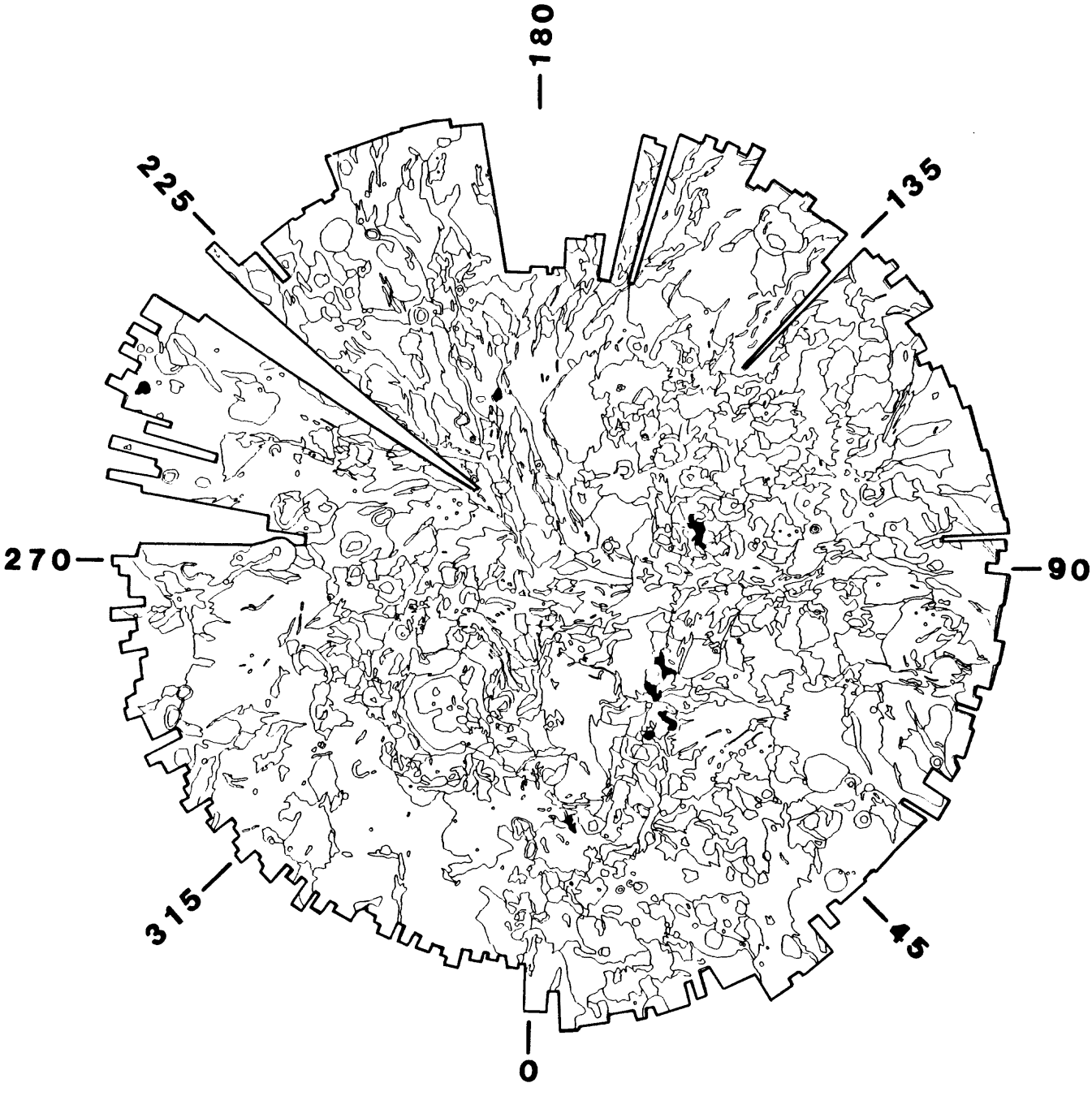

Fig. 11

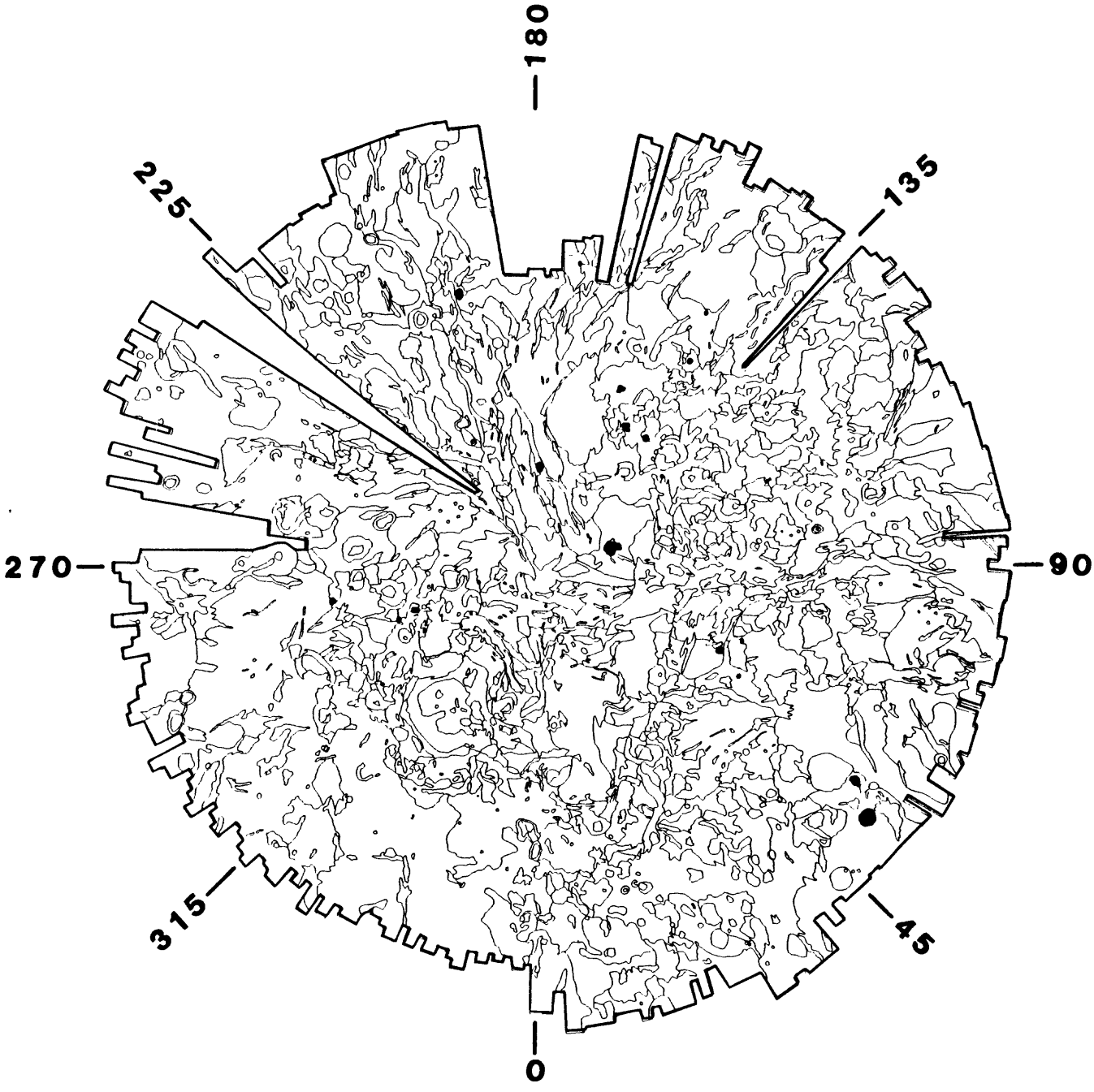

Fig, 12

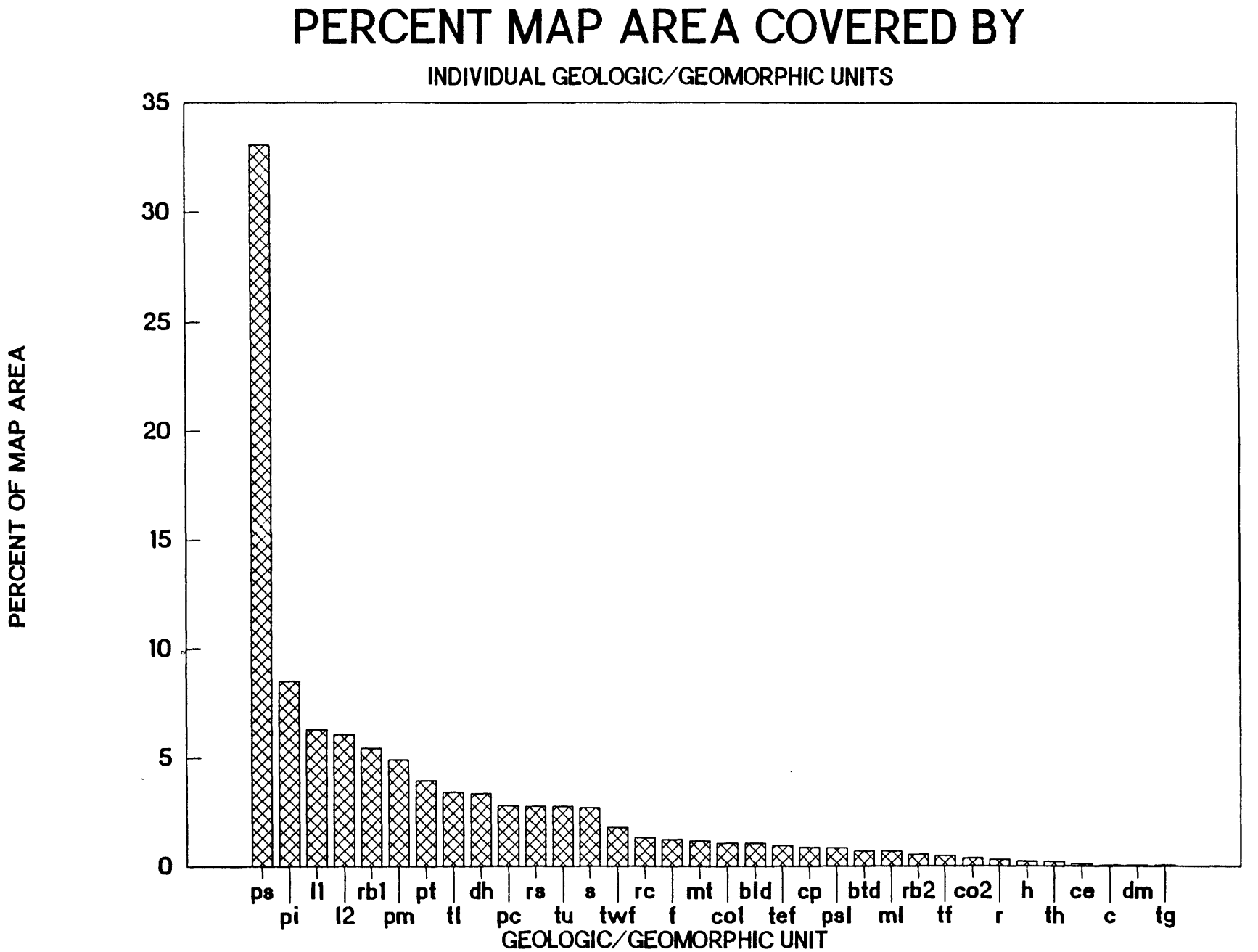
PERCENT MAP AREA COVERED BY
INDIVIDUAL GEOLOGIC/GEOMORPHIC UNITS
PERCENT OF MAP AREA
35
30
25
20
15
10
5
0
ps
pi
l1
l2
rb1
pm
pt
tl
dh
pc
rs
tu
s
twf
rc
f
mt
col
bld
tef
cp
psl
btd
ml
rb2
tf
co2
r
h
th
ce
c
dm
tg
GEOLOGIC/GEOMORPHIC UNIT

Fig. 13

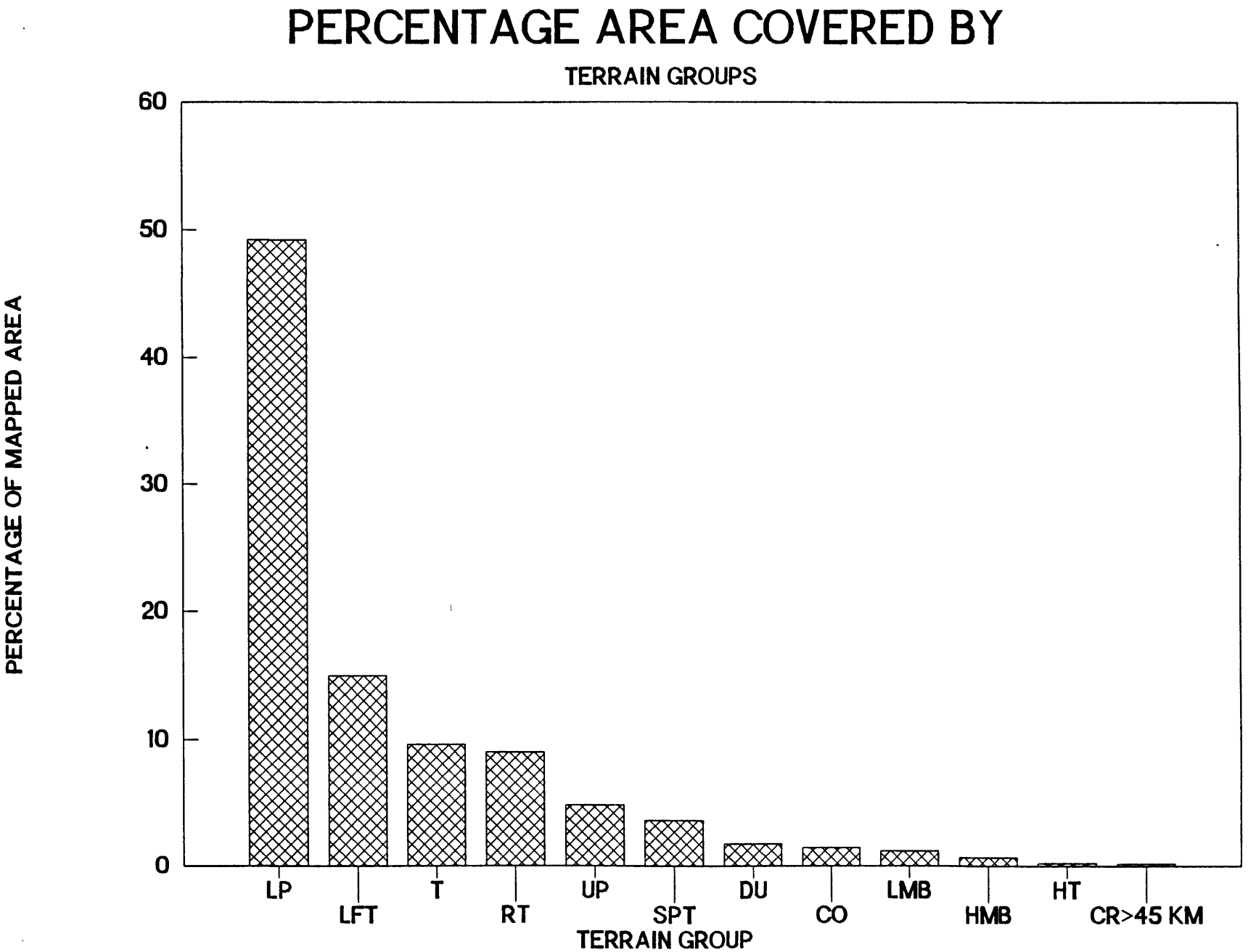
PERCENTAGE AREA COVERED BY
TERRAIN GROUPS
PERCENTAGE OF MAPPED AREA
60
50
40
30
20
10
0
LP
LFT
T
RT
UP
SPT
DU
CO
LMB
HMB
HT
CR>45 KM
TERRAIN GROUP

Fig. 14

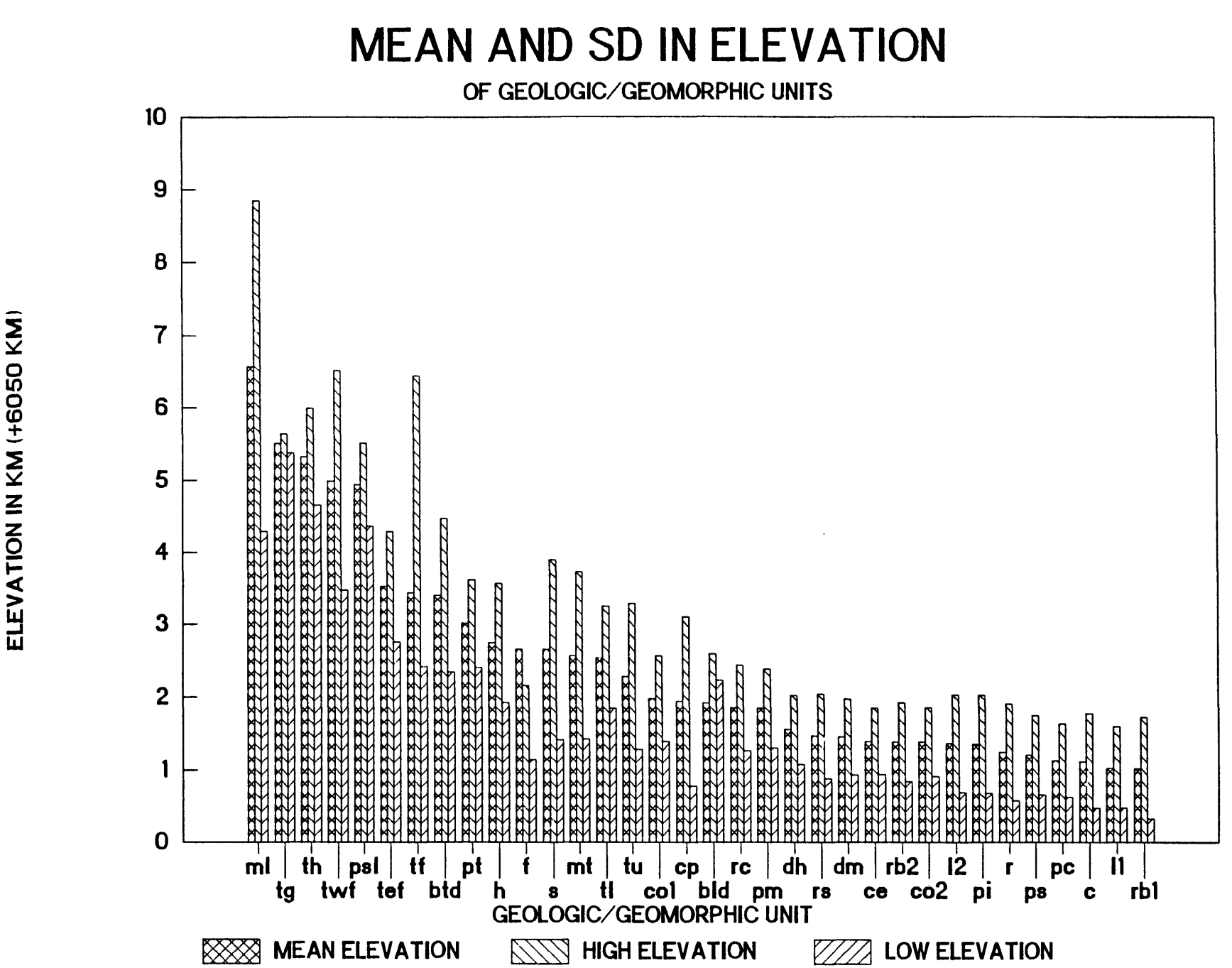
MEAN AND SD IN ELEVATION
OF GEOLOGIC/GEOMORPHIC UNITS
ELEVATION IN KM (+6050 KM)
10
9
8
7
6
5
4
3
2
1
0
ml
tg
th
twf
psl
tef
tf
btd
pt
h
f
s
mt
tl
tu
col
cp
bld
rc
pm
dh
rs
dm
ce
rb2
co2
l2
pi
r
ps
pc
c
l1
rbl
GEOLOGIC/GEOMORPHIC UNIT
MEAN ELEVATION
HIGH ELEVATION
LOW ELEVATION

Fig. 15

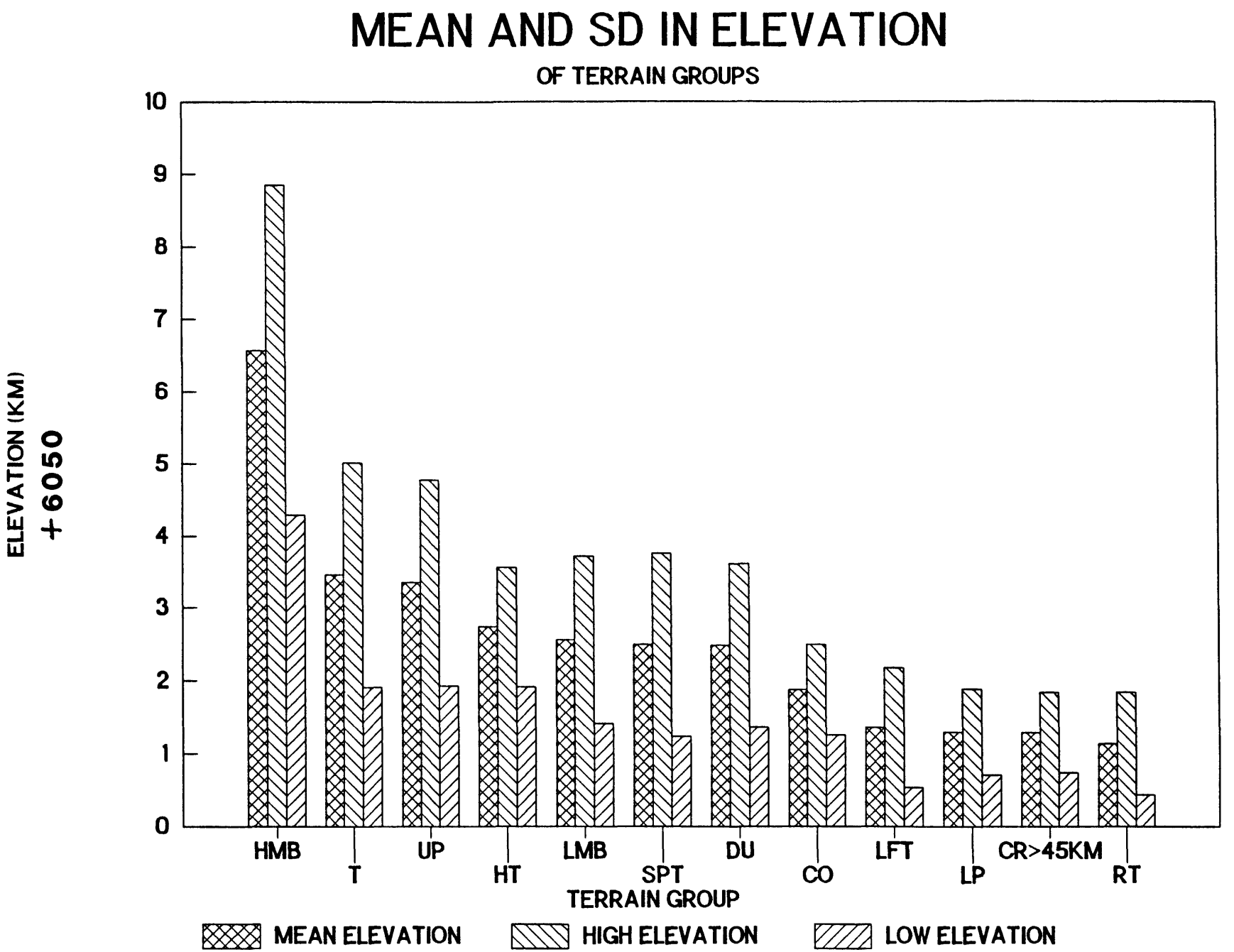
MEAN AND SD IN ELEVATION
OF TERRAIN GROUPS
ELEVATION (KM)
+6050
10
9
8
7
6
5
4
3
2
1
0
HMB
T
UP
HT
LMB
SPT
DU
CO
LFT
LP
CR>45KM
RT
TERRAIN GROUP
MEAN ELEVATION
HIGH ELEVATION
LOW ELEVATION

Fig. 16

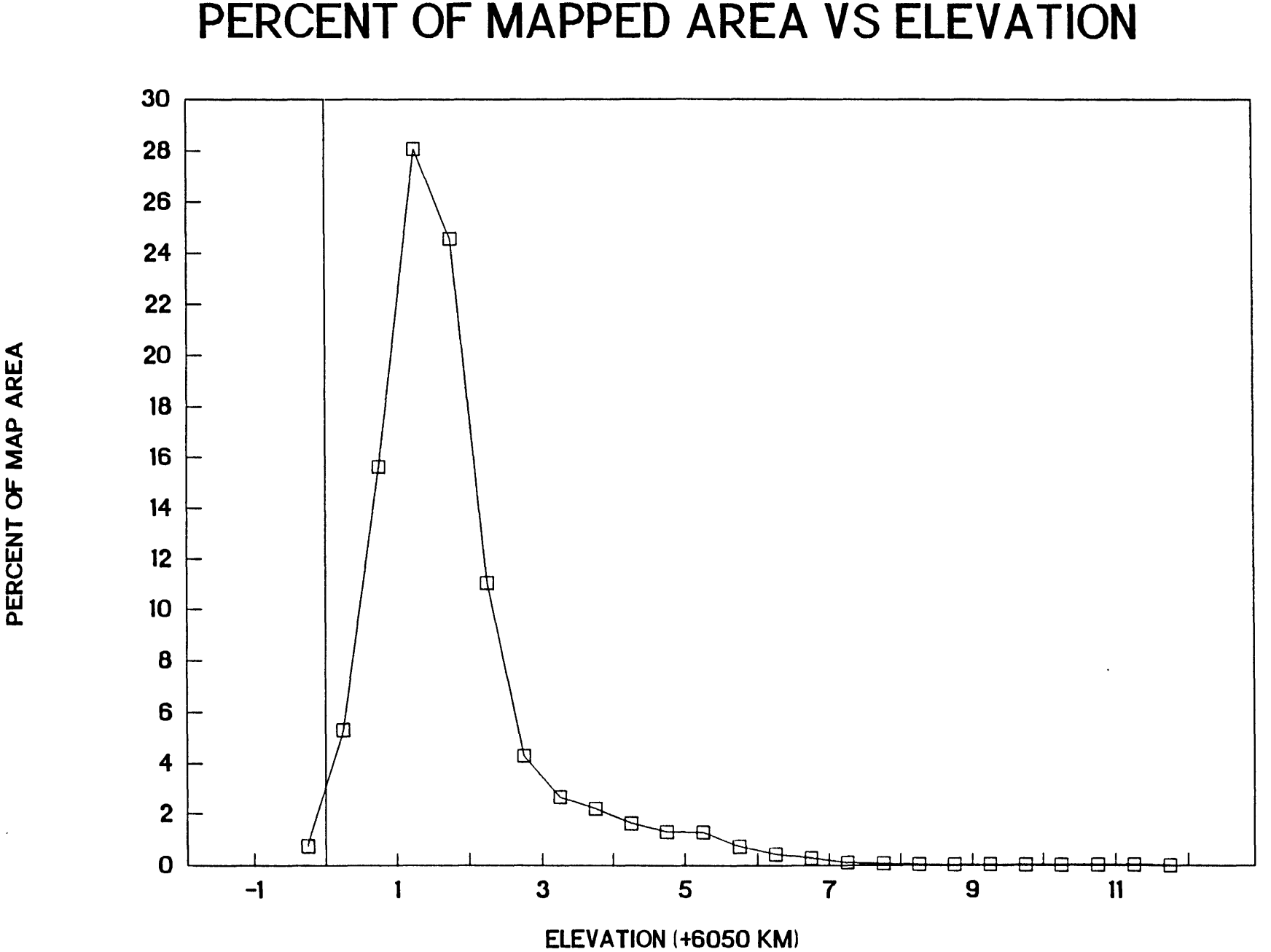
PERCENT OF MAPPED AREA VS ELEVATION
PERCENT OF MAP AREA
30
28
26
24
22
20
18
16
14
12
10
8
6
4
2
0
-1
1
3
5
7
9
11
ELEVATION (+6050 KM)

Fig. 17

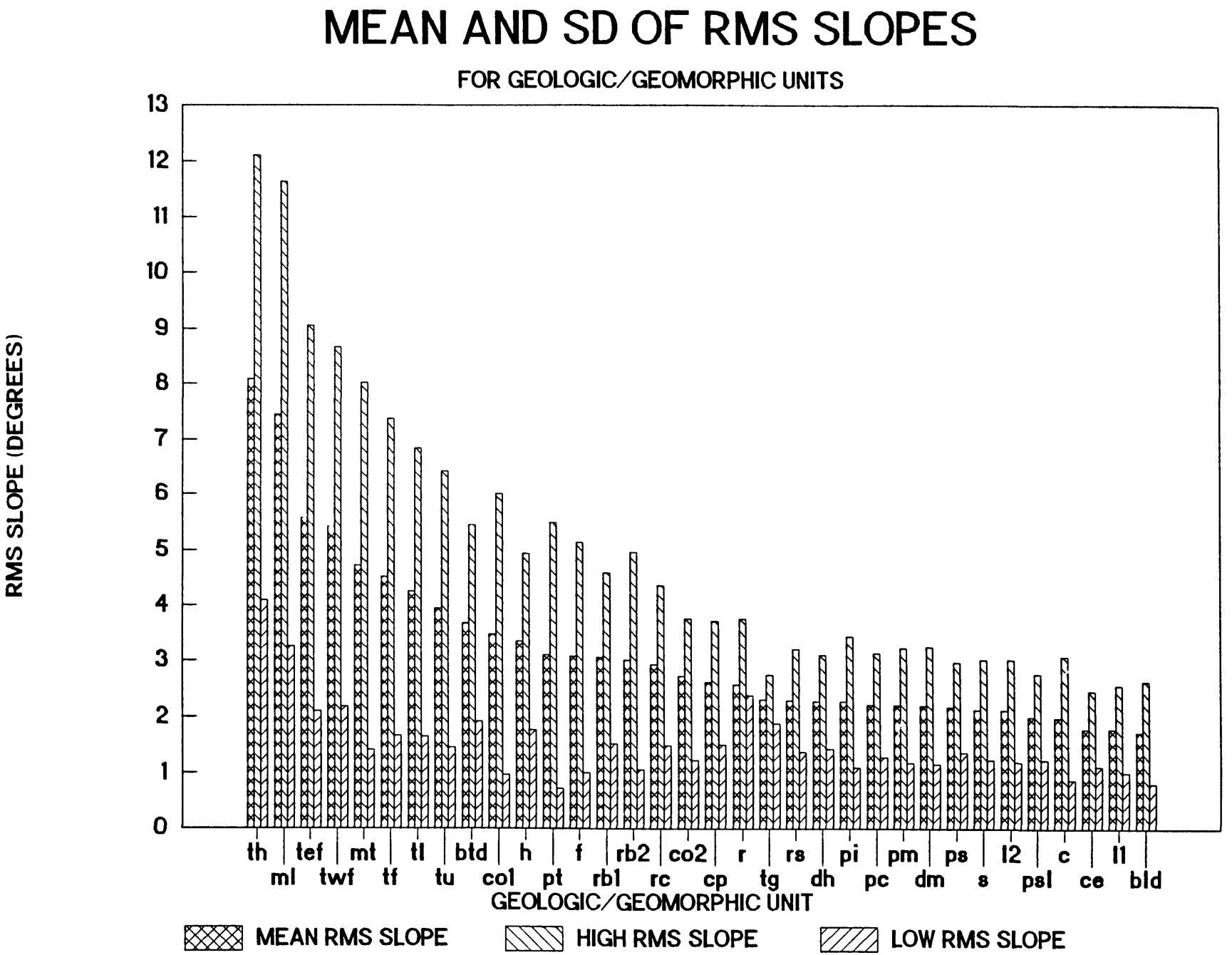
MEAN AND SD OF RMS SLOPES
FOR GEOLOGIC/GEOMORPHIC UNITS
RMS SLOPE (DEGREES)
0
1
2
3
4
5
6
7
8
9
10
11
12
13
th
tef
mt
tl
btd
h
f
rb2
co2
r
rs
pi
pm
ps
l2
c
l1
ml
twf
tf
tu
col
pt
rb1
rc
cp
tg
dh
pc
dm
s
psl
ce
bld
GEOLOGIC/GEOMORPHIC UNIT
MEAN RMS SLOPE
HIGH RMS SLOPE
LOW RMS SLOPE

Fig. 18

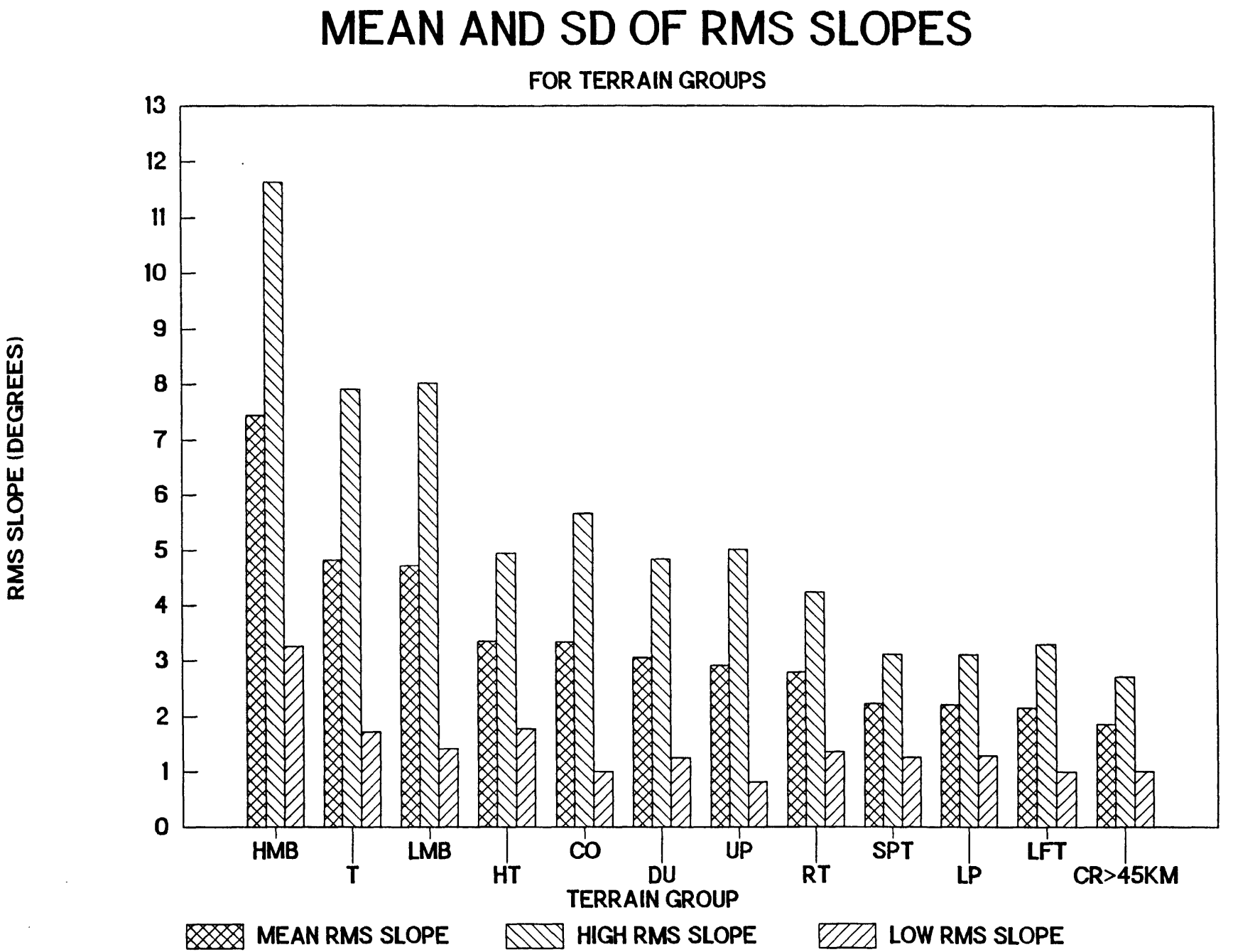
MEAN AND SD OF RMS SLOPES
FOR TERRAIN GROUPS
RMS SLOPE (DEGREES)
13
12
11
10
9
8
7
6
5
4
3
2
1
0
HMB
T
LMB
HT
CO
DU
UP
RT
SPT
LP
LFT
CR>45KM
TERRAIN GROUP
MEAN RMS SLOPE
HIGH RMS SLOPE
LOW RMS SLOPE

Fig. 19

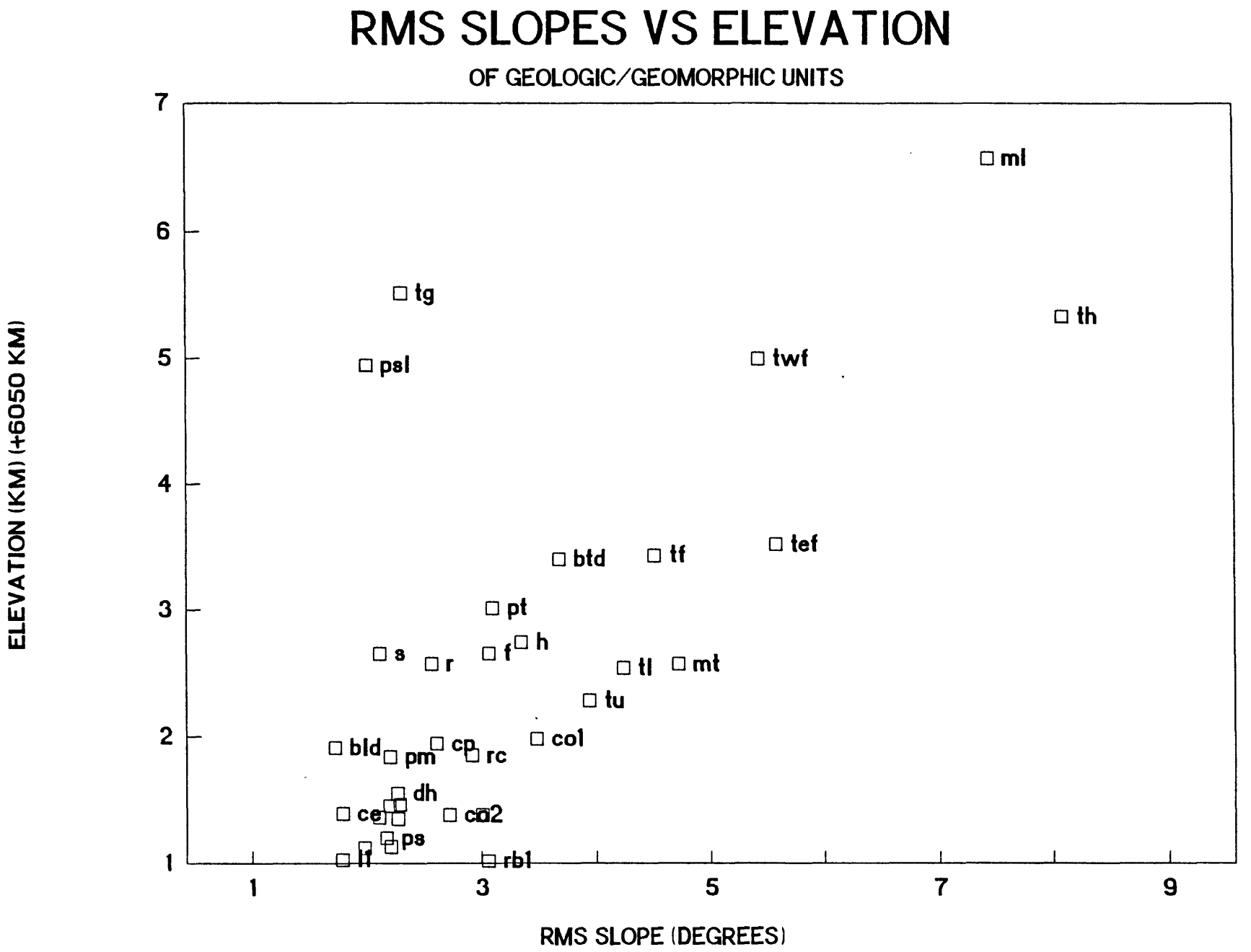
RMS SLOPES VS ELEVATION
OF GEOLOGIC/GEOMORPHIC UNITS
ELEVATION (KM) (+6050 KM)
RMS SLOPE (DEGREES)
7
6
5
4
3
2
1
1
3
5
7
9
ml
th
tg
psl
twf
tef
btd
tf
pt
h
s
r
f
tl
mt
tu
bld
pm
cp
rc
col
dh
ce
co2
ps
lf
rbl

Fig. 20

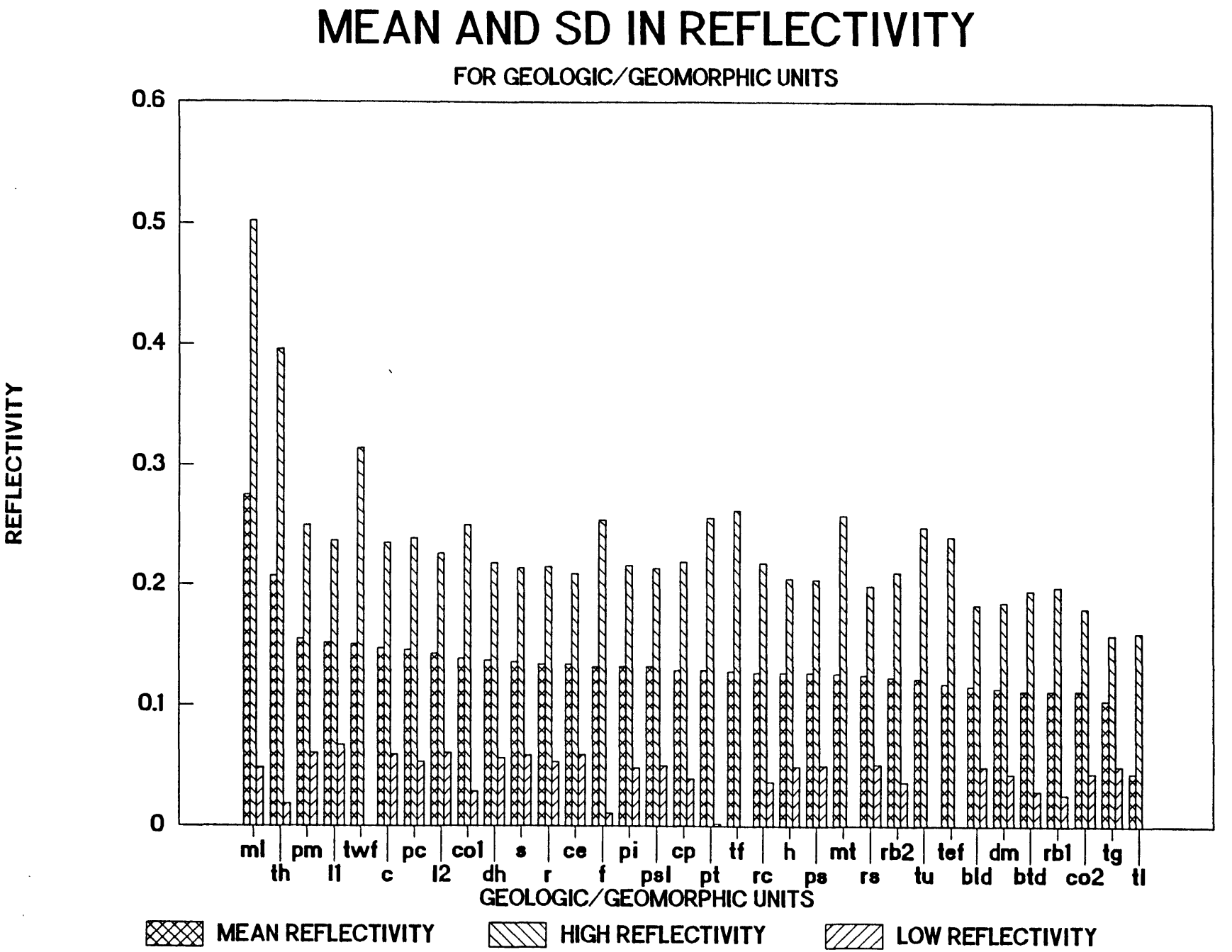
MEAN AND SD IN REFLECTIVITY
FOR GEOLOGIC/GEOMORPHIC UNITS
REFLECTIVITY
0.6
0.5
0.4
0.3
0.2
0.1
0
ml
th
pm
l1
twf
c
pc
l2
col
dh
s
r
ce
f
pi
psl
cp
pt
tf
rc
h
ps
mt
rs
rb2
tu
tef
bld
dm
btd
rb1
co2
tg
tl
GEOLOGIC/GEOMORPHIC UNITS
MEAN REFLECTIVITY
HIGH REFLECTIVITY
LOW REFLECTIVITY

Fig. 21

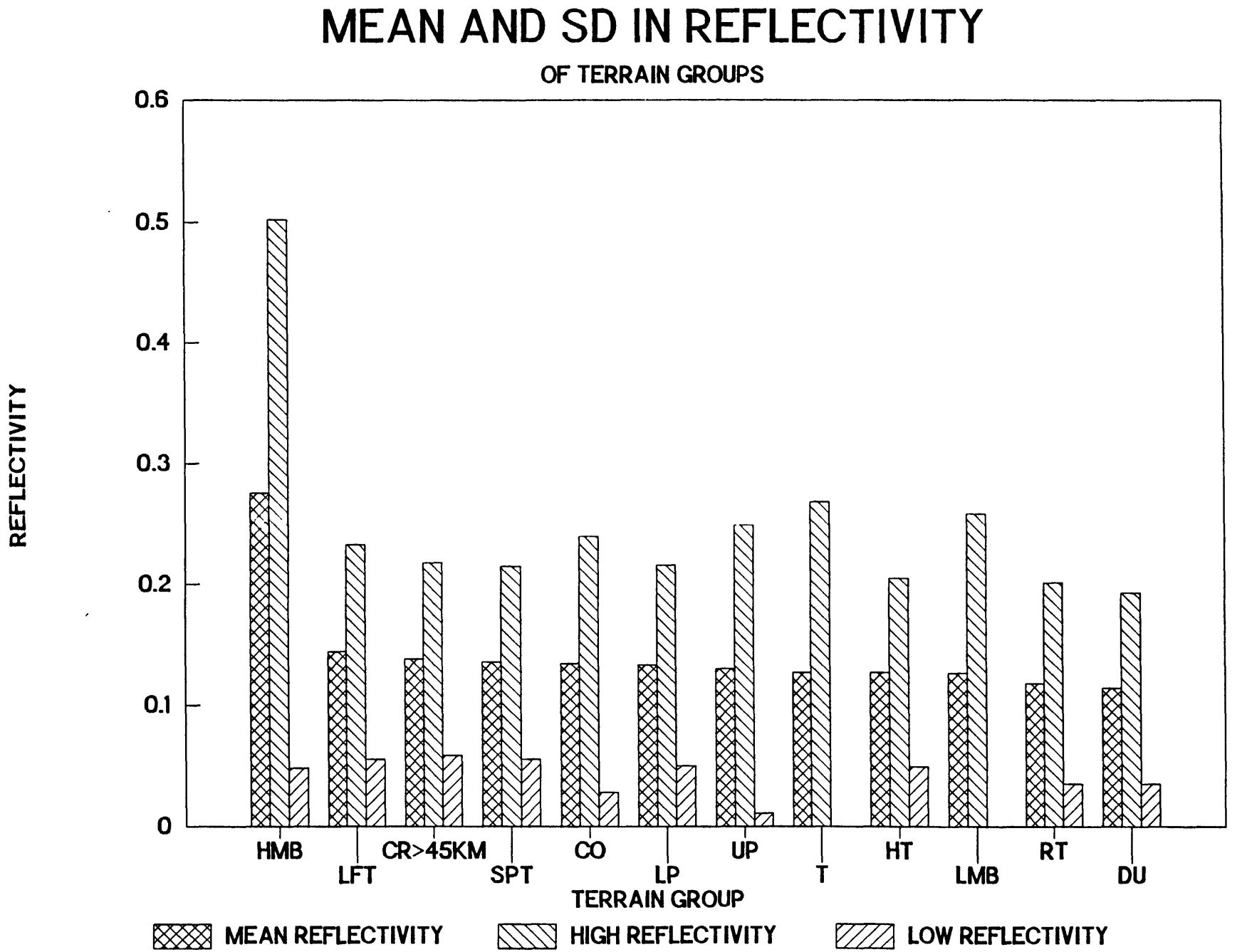
MEAN AND SD IN REFLECTIVITY
OF TERRAIN GROUPS
REFLECTIVITY
0.6
0.5
0.4
0.3
0.2
0.1
0
HMB
LFT
CR>45KM
SPT
CO
LP
UP
T
HT
LMB
RT
DU
TERRAIN GROUP
MEAN REFLECTIVITY
HIGH REFLECTIVITY
LOW REFLECTIVITY

Fig. 22

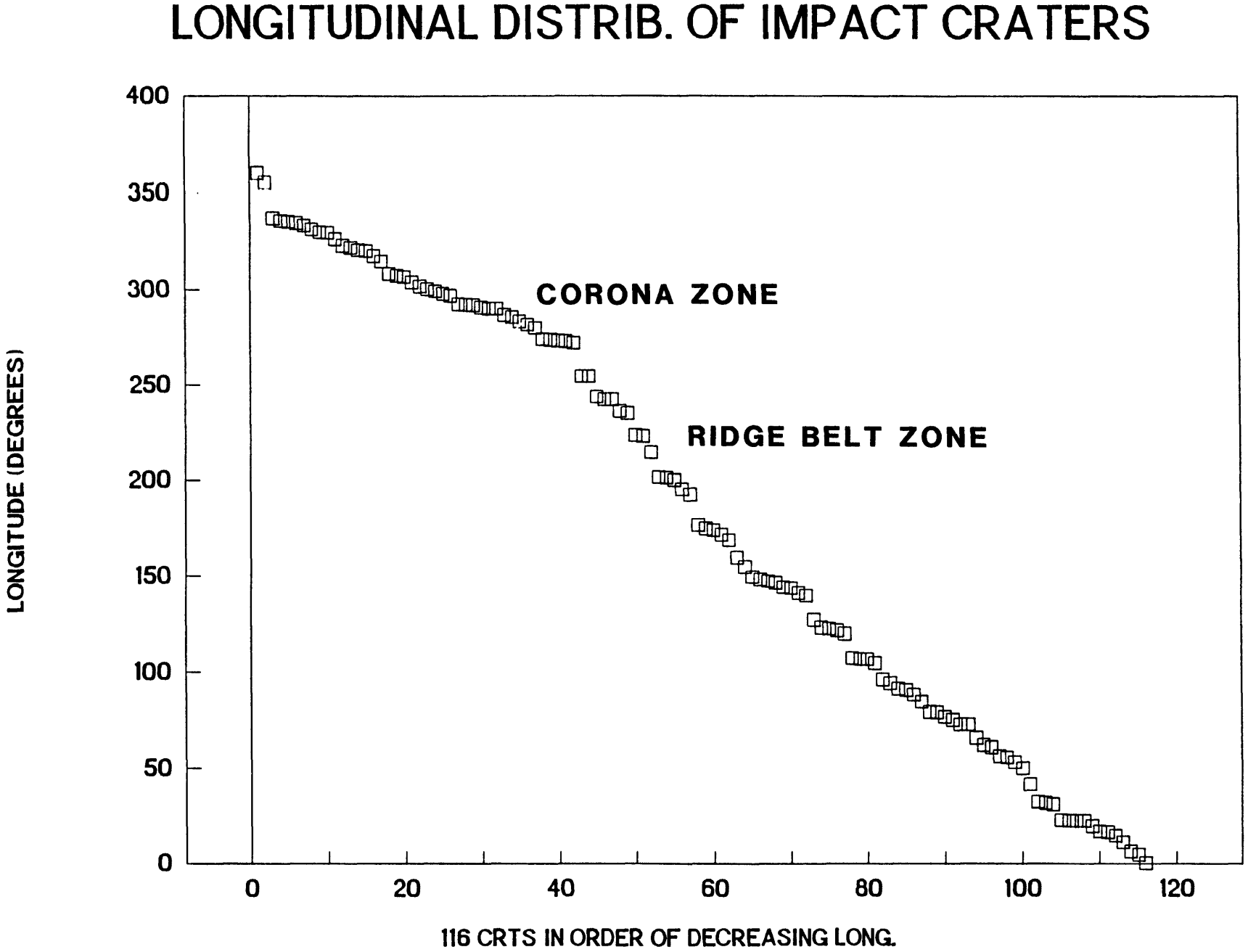
LONGITUDINAL DISTRIB. OF IMPACT CRATERS
LONGITUDE (DEGREES)
400
350
300
250
200
150
100
50
0
CORONA ZONE
RIDGE BELT ZONE
0
20
40
60
80
100
120
116 CRTS IN ORDER OF DECREASING LONG.

Fig. 23

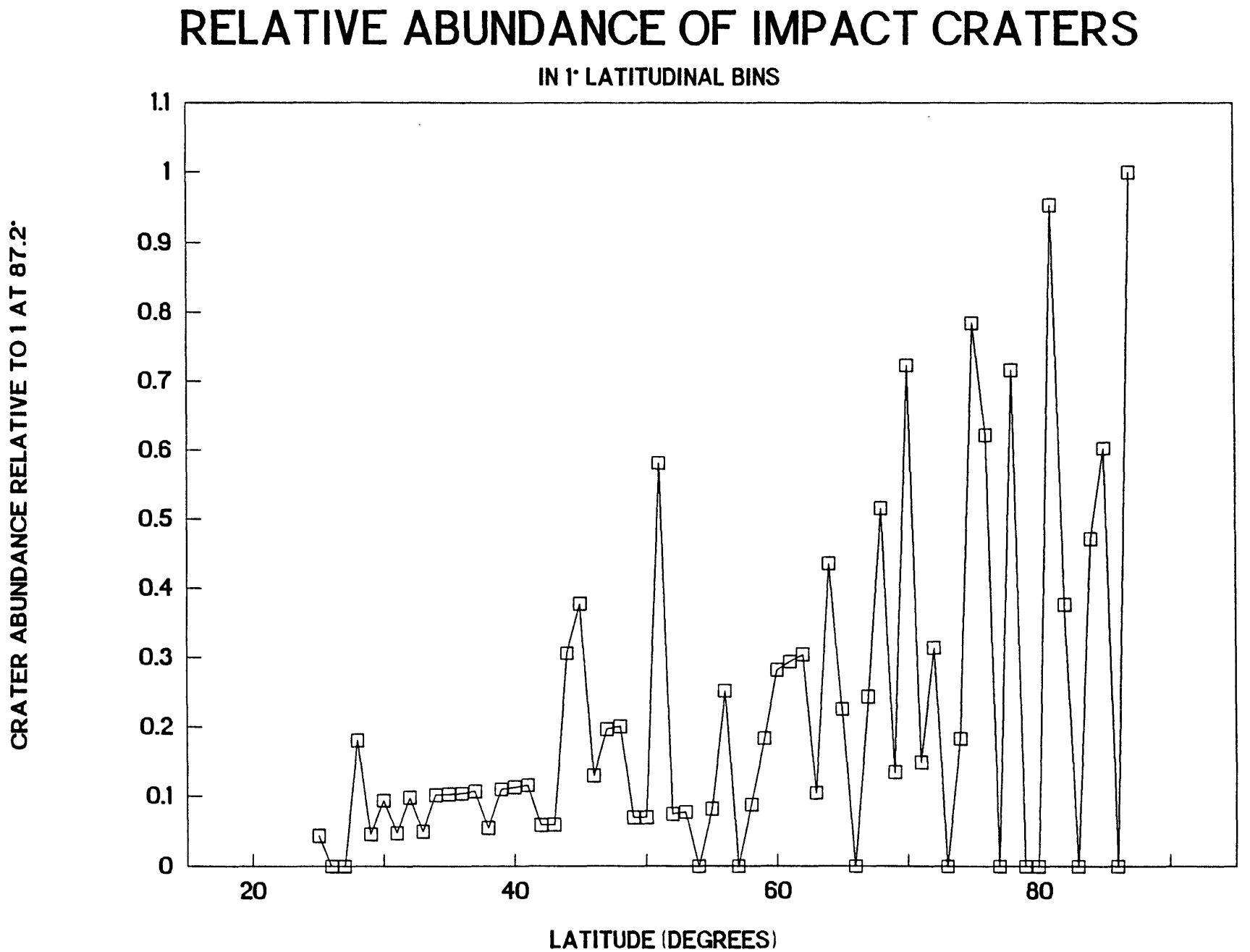
RELATIVE ABUNDANCE OF IMPACT CRATERS
IN 1° LATITUDINAL BINS
CRATER ABUNDANCE RELATIVE TO 1 AT 87.2°
1.1
1
0.9
0.8
0.7
0.6
0.5
0.4
0.3
0.2
0.1
0
20
40
60
80
LATITUDE (DEGREES)

Fig. 24

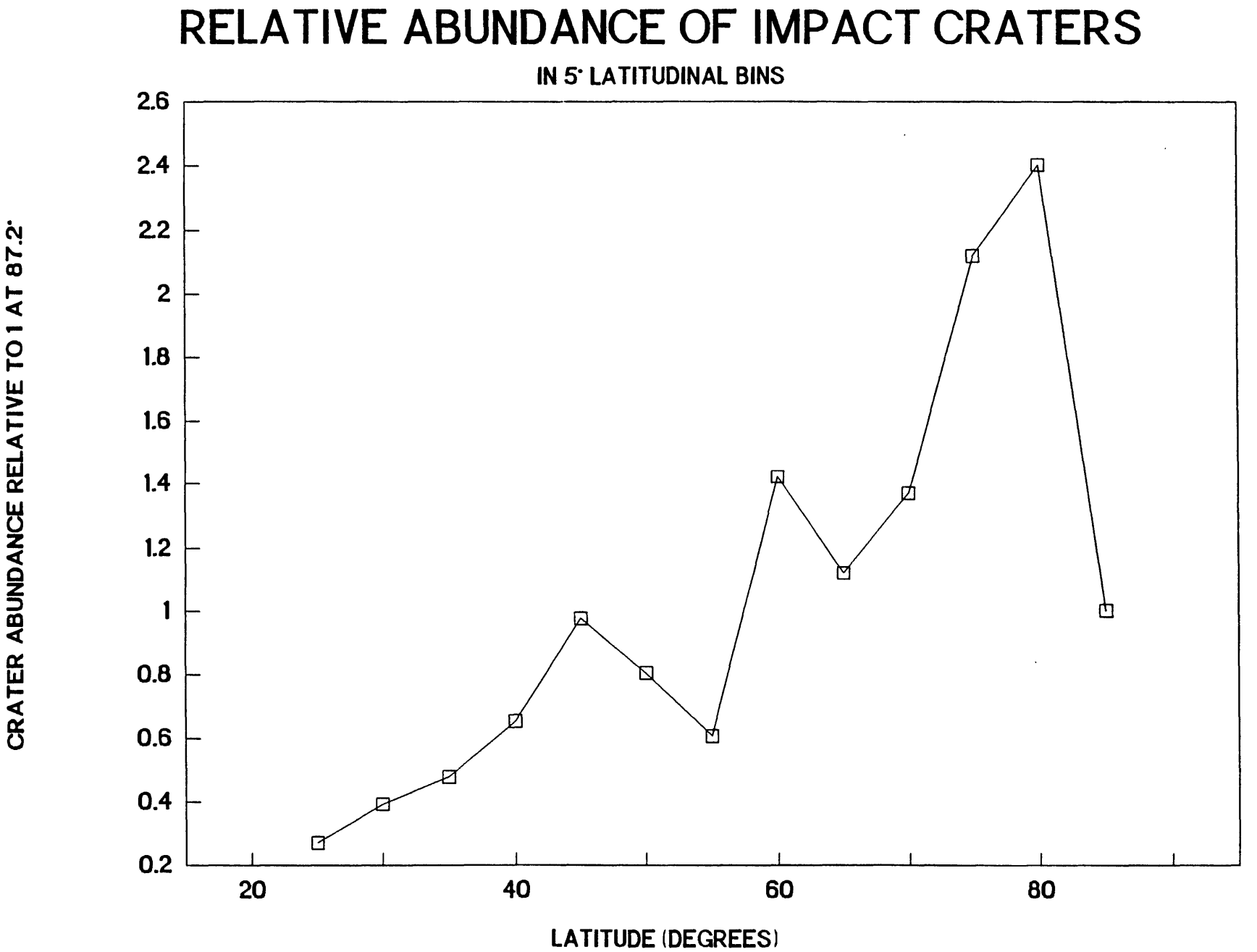
RELATIVE ABUNDANCE OF IMPACT CRATERS
IN 5° LATITUDINAL BINS
CRATER ABUNDANCE RELATIVE TO 1 AT 87.2°
2.6
2.4
2.2
2
1.8
1.6
1.4
1.2
1
0.8
0.6
0.4
0.2
20
40
60
80
LATITUDE (DEGREES)

Fig. 25

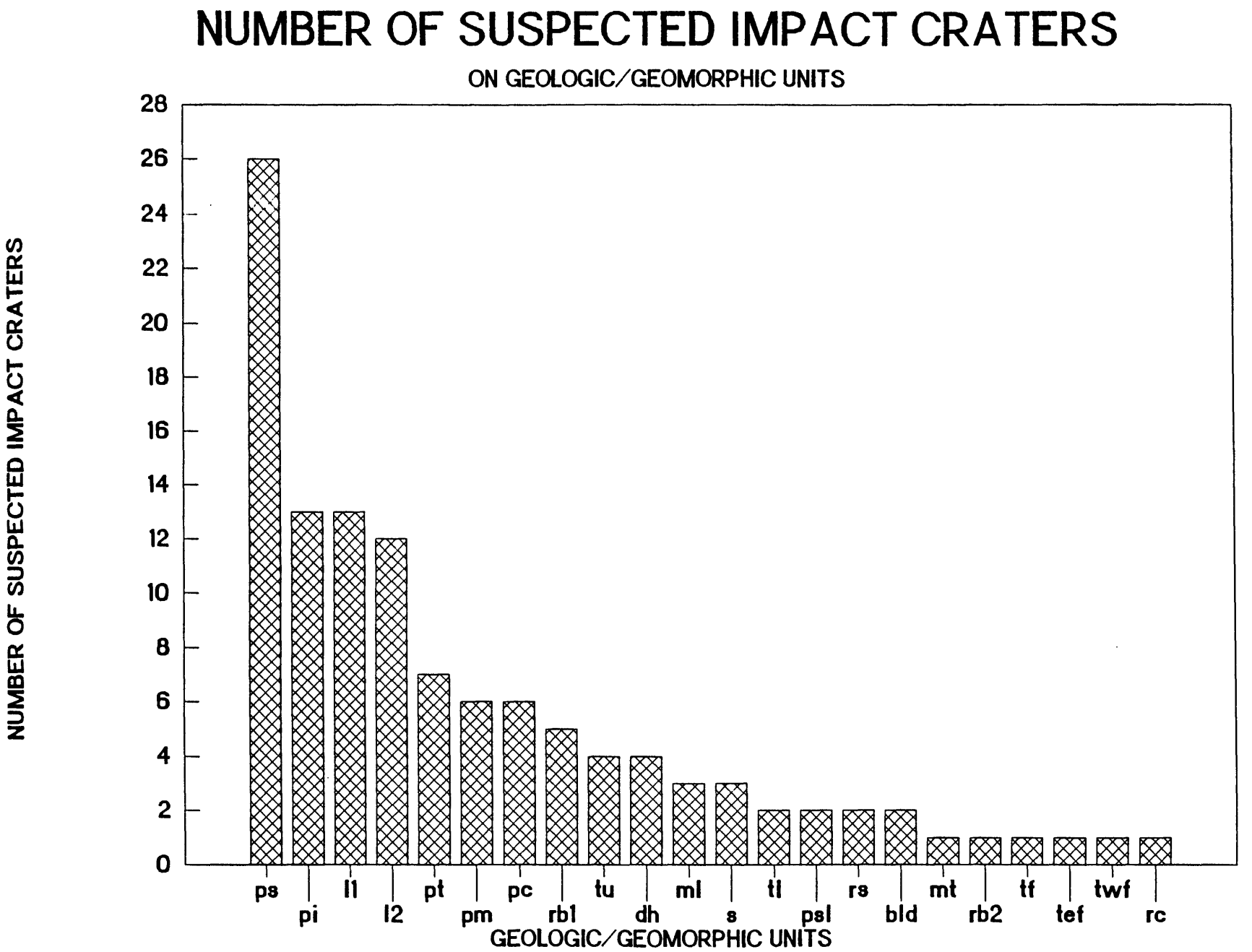
NUMBER OF SUSPECTED IMPACT CRATERS
ON GEOLOGIC/GEOMORPHIC UNITS
NUMBER OF SUSPECTED IMPACT CRATERS
28
26
24
22
20
18
16
14
12
10
8
6
4
2
0
ps
pi
l1
l2
pt
pm
pc
rb1
tu
dh
ml
s
tl
psl
rs
bld
mt
rb2
tf
tef
twf
rc
GEOLOGIC/GEOMORPHIC UNITS

Fig. 26

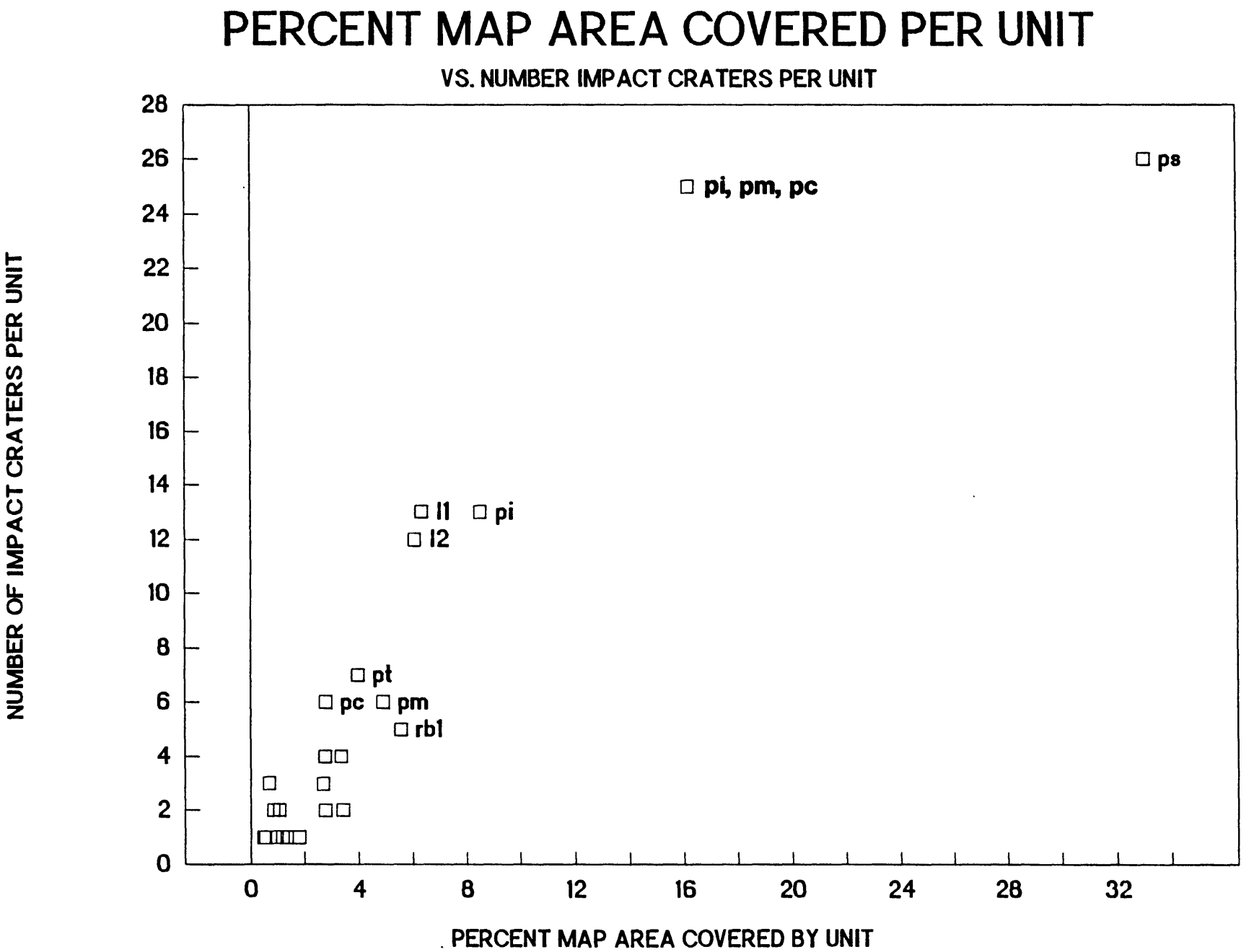
PERCENT MAP AREA COVERED PER UNIT
VS. NUMBER IMPACT CRATERS PER UNIT
NUMBER OF IMPACT CRATERS PER UNIT
PERCENT MAP AREA COVERED BY UNIT
0
2
4
6
8
10
12
14
16
18
20
22
24
26
28
0
4
8
12
16
20
24
28
32
ps
pi, pm, pc
l1
pi
l2
pt
pc
pm
rbl

Fig. 27

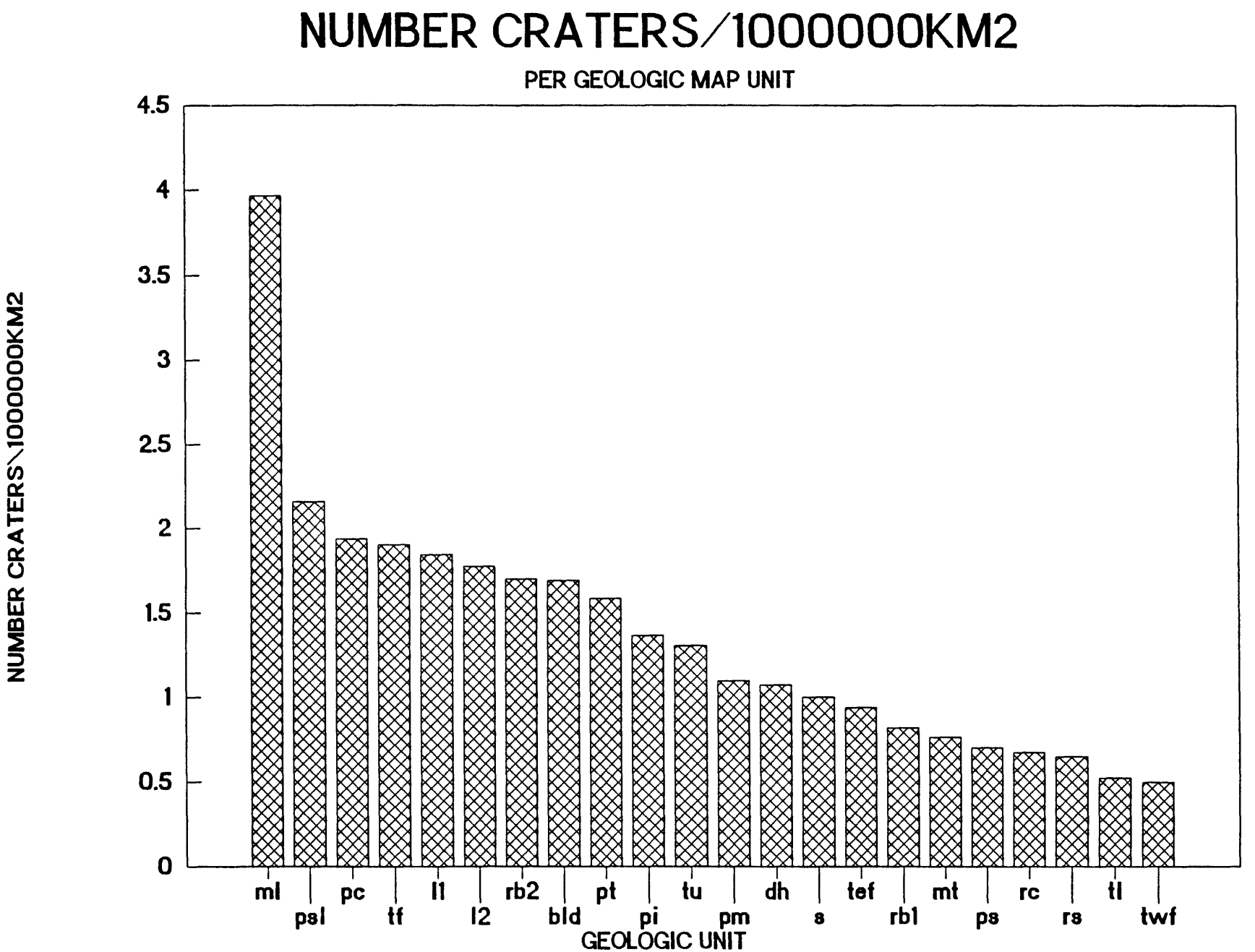
NUMBER CRATERS/1000000KM2
PER GEOLOGIC MAP UNIT
NUMBER CRATERS\1000000KM2
4.5
4
3.5
3
2.5
2
1.5
1
0.5
0
ml
psl
pc
tf
l1
l2
rb2
bld
pt
pi
tu
pm
dh
s
tef
rbl
mt
ps
rc
rs
tl
twf
GEOLOGIC UNIT

Fig. 28

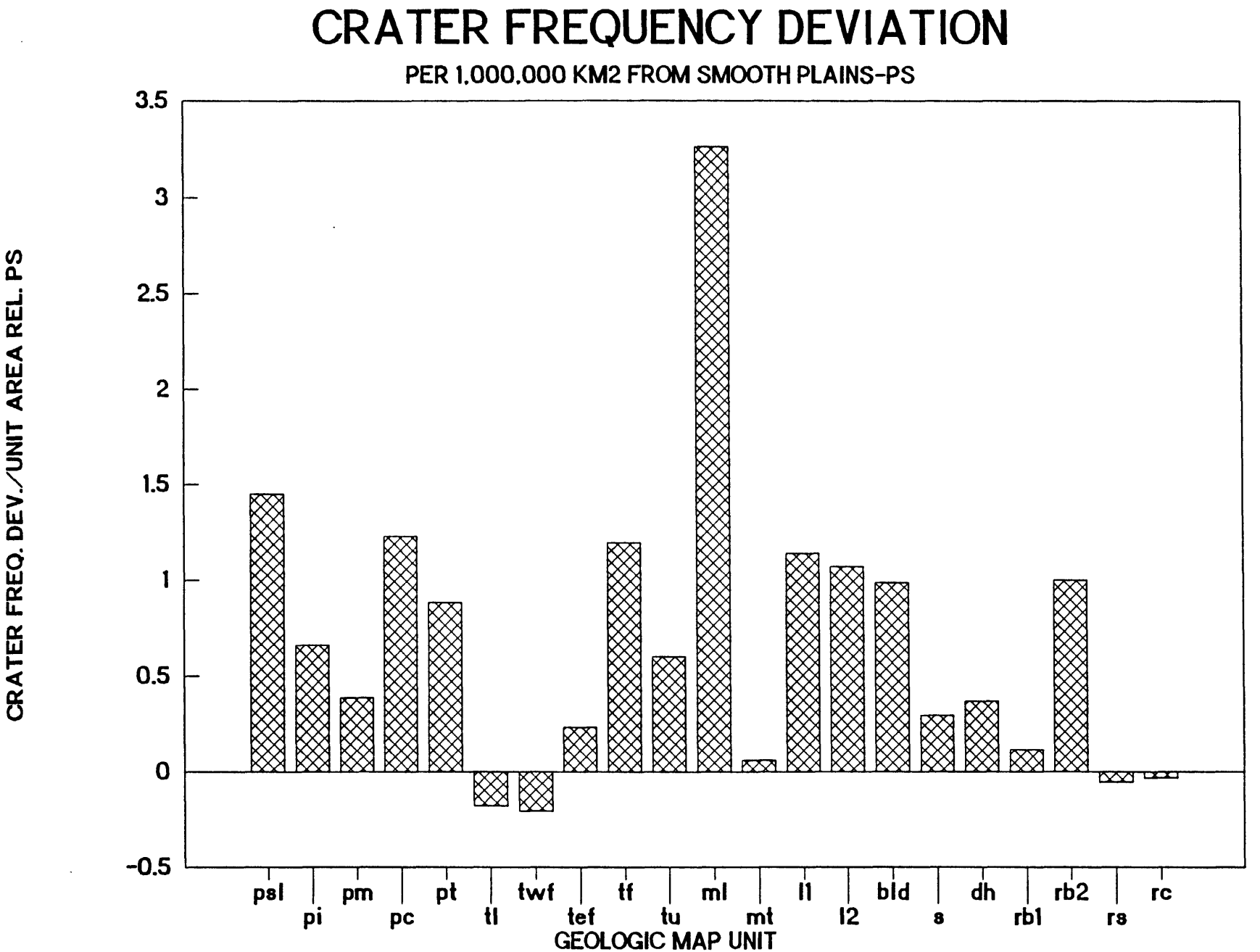
CRATER FREQUENCY DEVIATION
PER 1,000,000 KM2 FROM SMOOTH PLAINS-PS
CRATER FREQ. DEV./UNIT AREA REL. PS
3.5
3
2.5
2
1.5
1
0.5
0
-0.5
psl
pi
pm
pc
pt
tl
twf
tef
tf
tu
ml
mt
l1
l2
bld
s
dh
rb1
rb2
rs
rc
GEOLOGIC MAP UNIT

Fig. 29

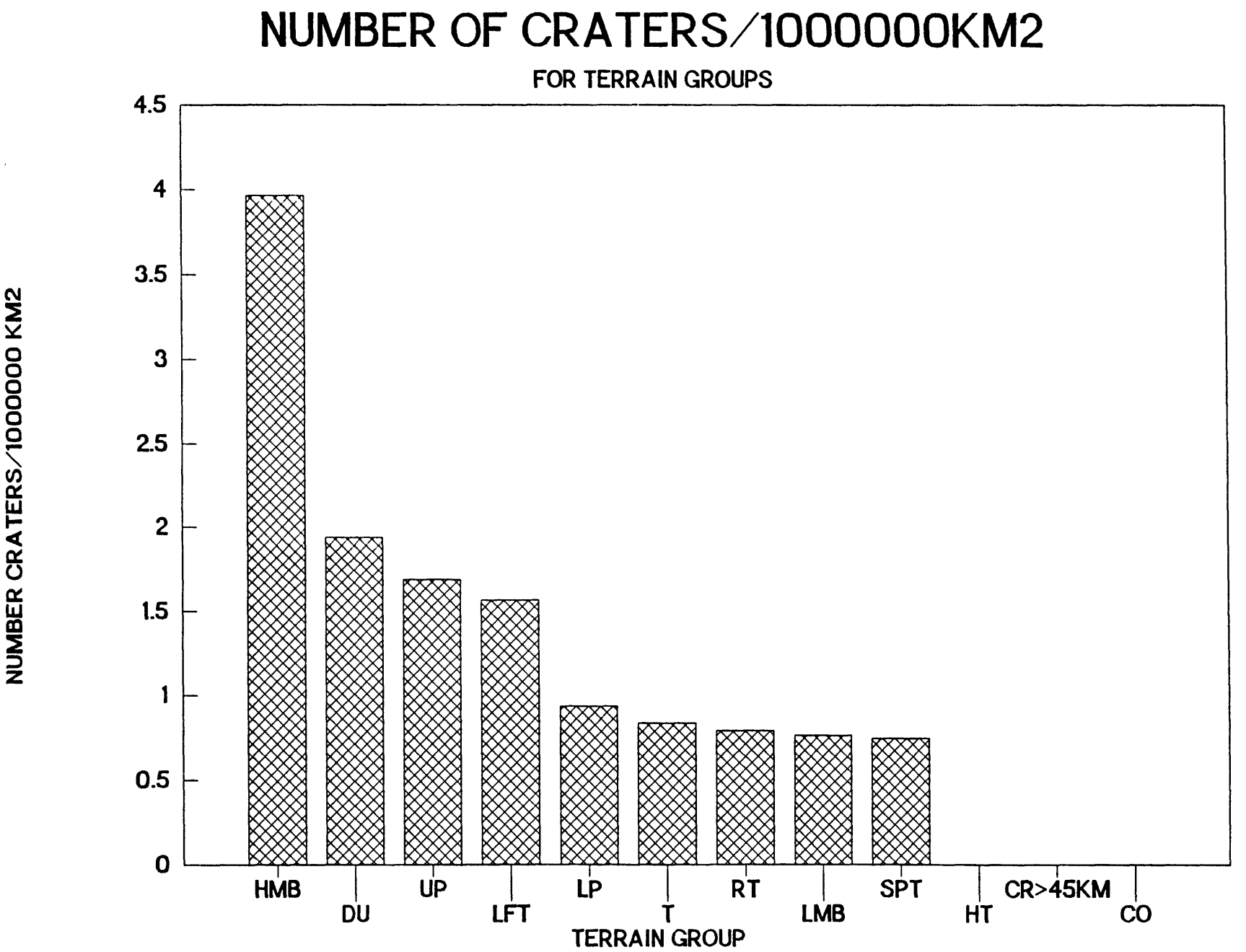
NUMBER OF CRATERS/1000000KM2
FOR TERRAIN GROUPS
NUMBER CRATERS/1000000 KM2
4.5
4
3.5
3
2.5
2
1.5
1
0.5
0
HMB
DU
UP
LFT
LP
T
RT
LMB
SPT
HT
CR>45KM
CO
TERRAIN GROUP

Fig. 30

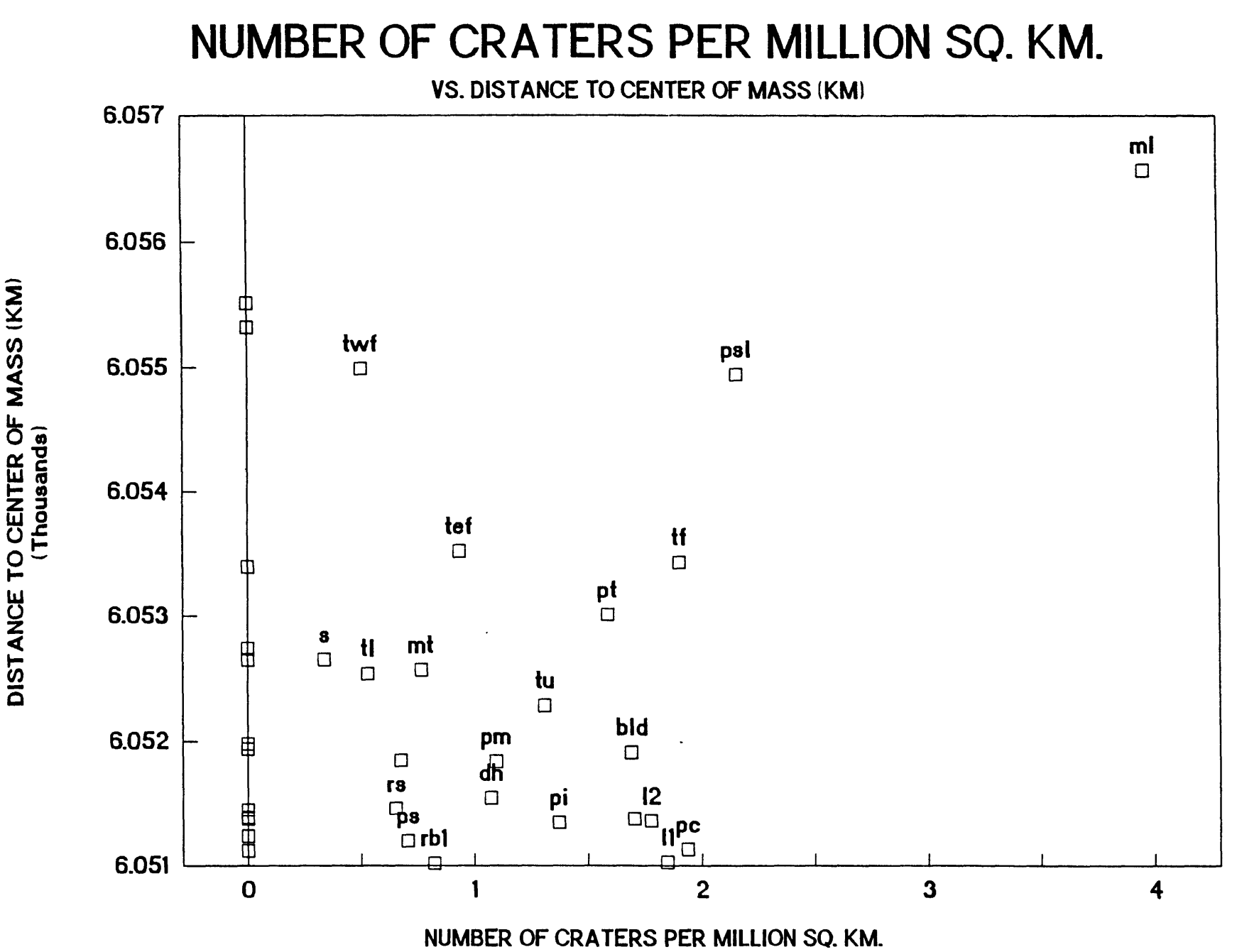
NUMBER OF CRATERS PER MILLION SQ. KM.
VS. DISTANCE TO CENTER OF MASS (KM)
DISTANCE TO CENTER OF MASS (KM)
(Thousands)
6.057
6.056
6.055
6.054
6.053
6.052
6.051
0
1
2
3
4
NUMBER OF CRATERS PER MILLION SQ. KM.
ml
twf
psl
tef
tf
pt
s
tl
mt
tu
bld
pm
dh
rs
pi
l2
ps
rbl
l1
pc

Fig. 31

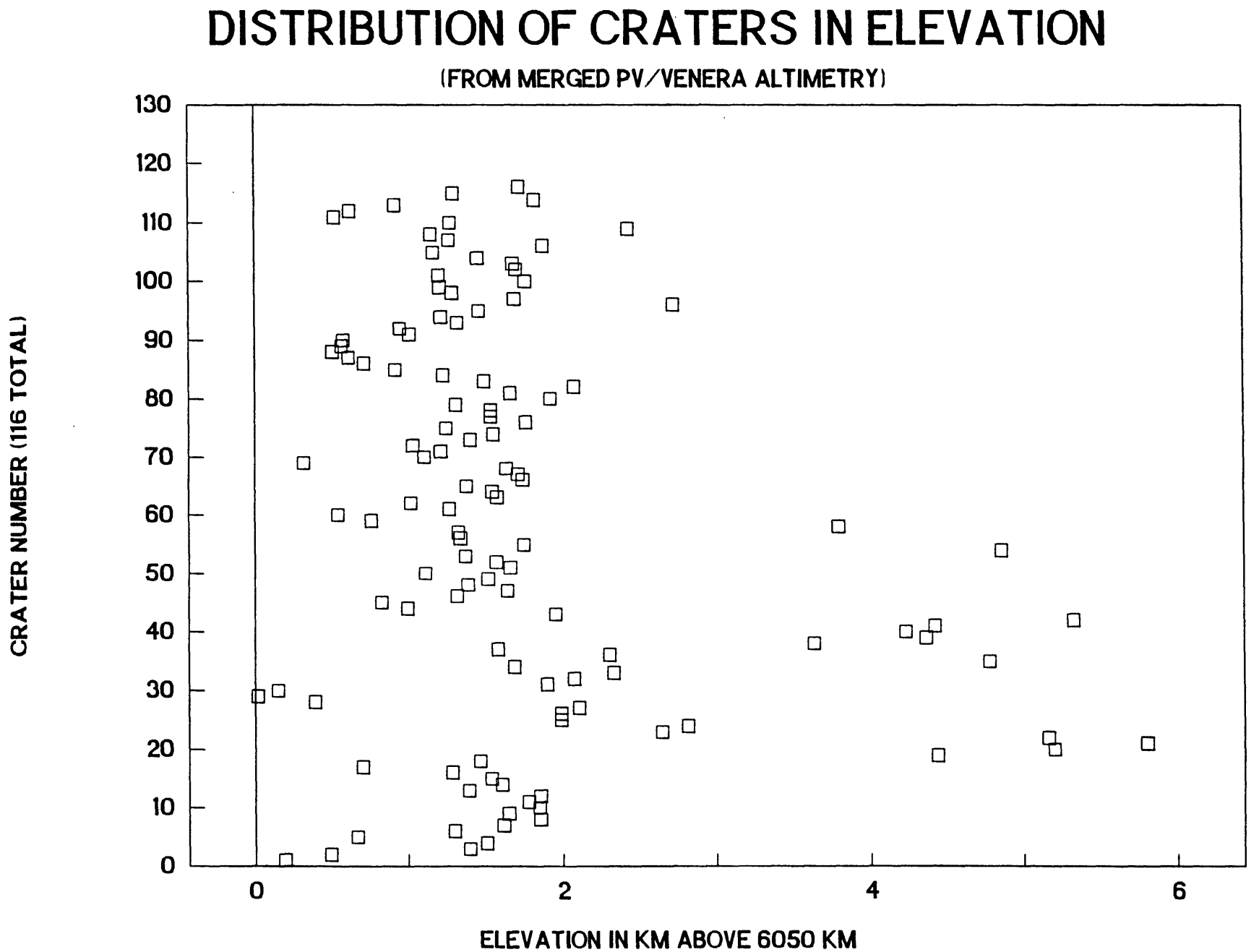
DISTRIBUTION OF CRATERS IN ELEVATION
(FROM MERGED PV/VENERA ALTIMETRY)
CRATER NUMBER (116 TOTAL)
130
120
110
100
90
80
70
60
50
40
30
20
10
0
0
2
4
6
ELEVATION IN KM ABOVE 6050 KM

Fig. 32

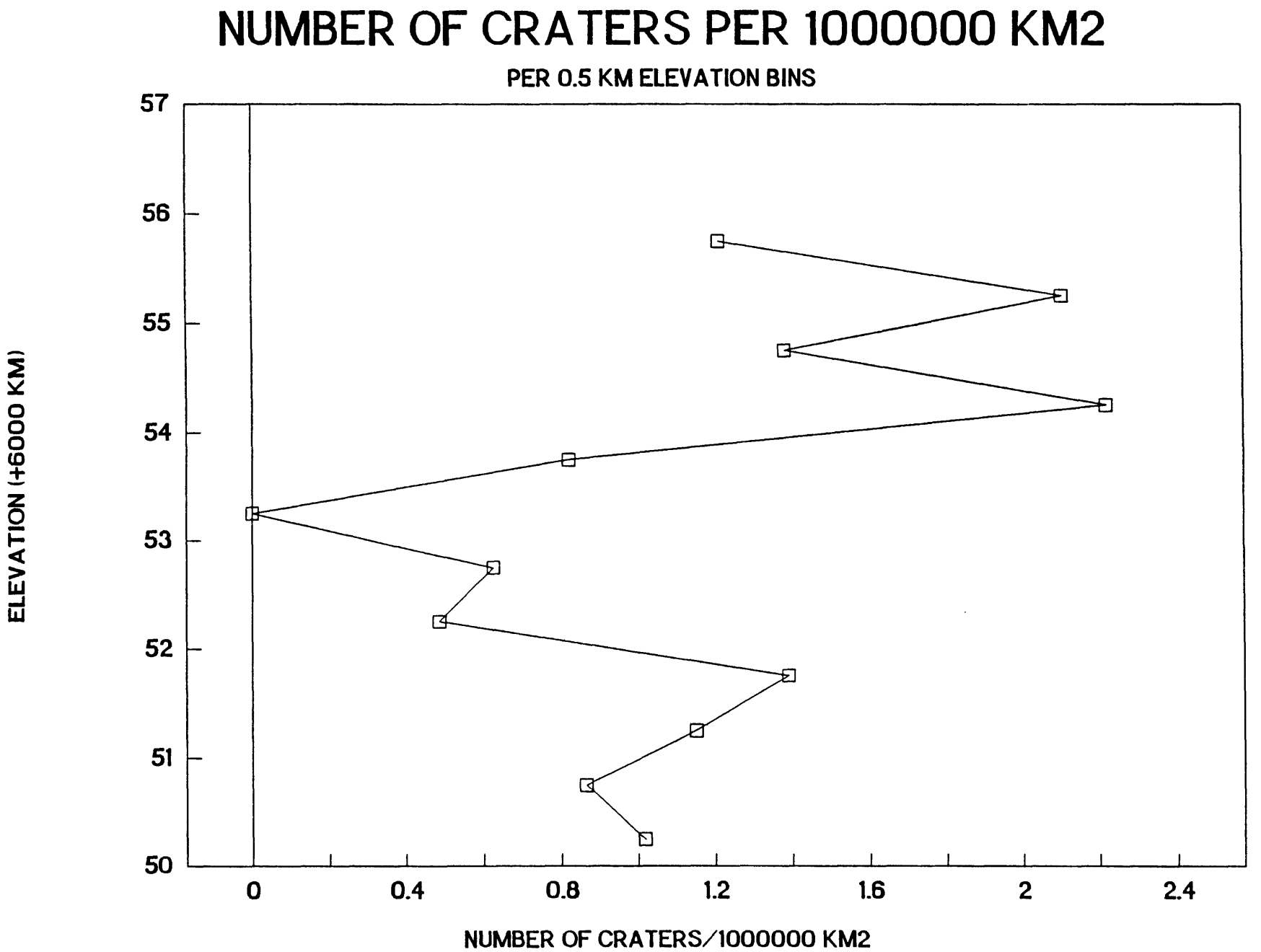
NUMBER OF CRATERS PER 1000000 KM2
PER 0.5 KM ELEVATION BINS
ELEVATION (+6000 KM)
57
56
55
54
53
52
51
50
0
0.4
0.8
1.2
1.6
2
2.4
NUMBER OF CRATERS/1000000 KM2

Fig. 33

CRATER DIAMETER VS. ELEVATION

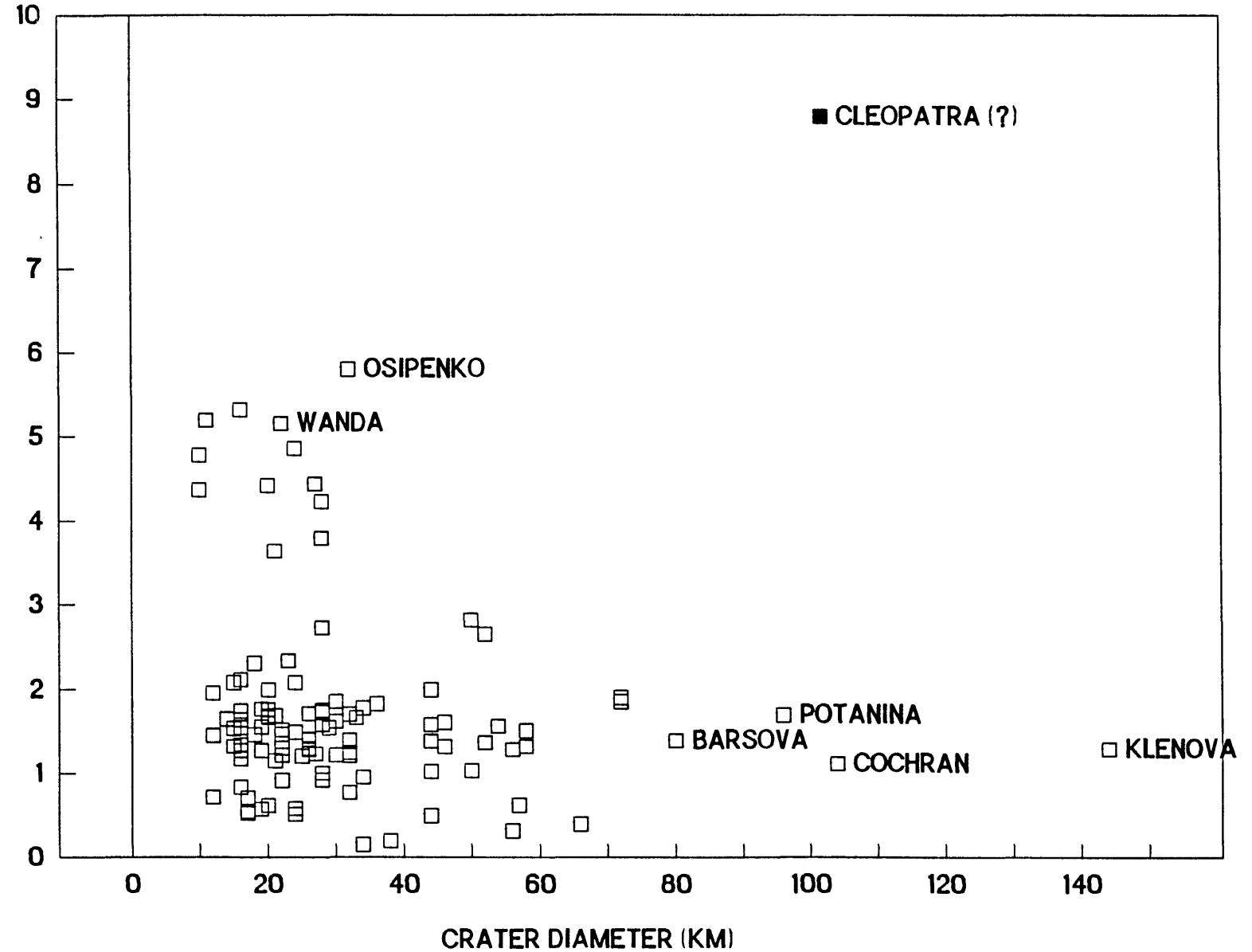

Fig. 34